

# Organic & Biomolecular Chemistry

Accepted Manuscript



This is an *Accepted Manuscript*, which has been through the Royal Society of Chemistry peer review process and has been accepted for publication.

*Accepted Manuscripts* are published online shortly after acceptance, before technical editing, formatting and proof reading. Using this free service, authors can make their results available to the community, in citable form, before we publish the edited article. We will replace this *Accepted Manuscript* with the edited and formatted *Advance Article* as soon as it is available.

You can find more information about *Accepted Manuscripts* in the [Information for Authors](#).

Please note that technical editing may introduce minor changes to the text and/or graphics, which may alter content. The journal's standard [Terms & Conditions](#) and the [Ethical guidelines](#) still apply. In no event shall the Royal Society of Chemistry be held responsible for any errors or omissions in this *Accepted Manuscript* or any consequences arising from the use of any information it contains.

**Recognition of double-stranded DNA using energetically activated duplexes with interstrand zippers of 1-, 2- or 4-pyrenyl-functionalized O2'-alkylated RNA monomers<sup>†</sup>**

Saswata Karmakar,<sup>a</sup> Andreas S. Madsen,<sup>b</sup> Dale C. Guenther,<sup>a</sup> Bradley C. Gibbons,<sup>a,c</sup> and Patrick J. Hrdlicka\*<sup>a</sup>

<sup>a</sup>Department of Chemistry, University of Idaho, Moscow, ID-83844, USA

<sup>b</sup>Department of Chemistry, Technical University of Denmark, Kemitorvet 207, Kgs. Lyngby, DK-2800, Denmark

<sup>c</sup>Department of Chemistry, Brigham Young University-Idaho, ID-83440, USA

\*Corresponding author: Tel: (+1) 208 885 0108. Fax: (+1) 208 885 6173. Email: [hrdlicka@uidaho.edu](mailto:hrdlicka@uidaho.edu).

**ABSTRACT.** Despite advances with triplex-forming oligonucleotides, peptide nucleic acids, polyamides and - more recently - engineered proteins, there remains an urgent need for synthetic ligands that enable specific recognition of double-stranded (ds) DNA to accelerate studies aiming at detecting, regulating and modifying genes. Invaders, i.e., energetically activated DNA duplexes with interstrand zipper arrangements of intercalator-functionalized nucleotides, are emerging as an attractive approach toward this goal. Here, we characterize and compare Invaders based on 1-, 2- and 4-pyrenyl-functionalized O2'-alkylated uridine monomers **X-Z** by means of thermal denaturation experiments, optical spectroscopy, force-field simulations and recognition experiments using DNA hairpins as model targets. We demonstrate that Invaders with +1 interstrand zippers of **X** or **Y** monomers efficiently recognize mixed-sequence DNA hairpins

with single nucleotide fidelity. Intercalator-mediated unwinding and activation of the double-stranded probe, coupled with extraordinary stabilization of probe-target duplexes ( $\Delta T_m$ /modification up to +14.0 °C), provides the driving force for dsDNA recognition. In contrast, **Z**-modified Invaders show much lower dsDNA recognition efficiency. Thus, even very conservative changes in the chemical makeup of the intercalator-functionalized nucleotides used to activate Invader duplexes, affects dsDNA-recognition efficiency of the probes, which highlights the importance of systematic structure-property studies. The insight from this study will guide future design of Invaders for applications in molecular biology and nucleic acid diagnostics.

**INTRODUCTION.** The right-handed DNA helix is one of the most fundamental structures in Nature due to its role as the carrier of genetic information. The two strands comprising the helix are held together through  $\pi$ - $\pi$  stacking interactions between neighboring nucleobases and hydrogen bonding between base pairs.<sup>1</sup> Development of synthetic ligands that are capable of decoding the sequence information contained within double-stranded DNA (dsDNA) has proven very challenging as the Watson-Crick base pairs are buried deeply within the duplex core and not readily accessible to exogenous agents. The most established dsDNA-targeting agents, i.e., pyrrole-imidazole polyamides,<sup>2</sup> engineered proteins<sup>3</sup> and triplex-forming oligonucleotides<sup>4</sup> or peptide nucleic acids (PNAs),<sup>5</sup> accordingly recognize chemical features that are accessible via one of the grooves instead.<sup>6</sup> While these strategies are attractive, they are not without limitations. For example, PNA-based approaches normally require low salinity conditions, while triplex-based approaches require targets with polypurine tracts. Approaches with more relaxed sequence requirements have been developed but they still require the presence of purine stretches, a

circumstance that may not be met at a target of interest.<sup>7</sup> Other strategies allow recognition of mixed-sequence target regions that are unusually accessible to exogenous agents, such as AT-rich cruciforms or transcription bubbles.<sup>8</sup>

Synthetic ligands that recognize mixed-sequence *B*-DNA via duplex invasion are attractive due to the predictability of Watson-Crick base-pairing rules. However, these approaches must overcome a steep energetic penalty since pre-existing base pairs of *B*-DNA must be broken prior to probe binding. Pseudocomplementary DNA (pcDNA), i.e., DNA duplexes featuring modified nucleobases that form weak base pairs with each other, while allowing hybridization to complementary DNA, recognize mixed-sequence target regions at *B*-DNA termini.<sup>9</sup> This strategy has been successfully extended to pcPNA, which recognize internal regions of mixed-sequence dsDNA.<sup>10</sup> However, the self-inhibitory effects observed at high pcPNA concentrations and the requirement for low salinity, pose potential limitations for pcPNA-mediated strand invasion in biological media.<sup>11</sup>  $\gamma$ -PNA, i.e., single-stranded probes that are fully modified with conformationally pre-organized PNA building blocks, are another interesting class of dsDNA-targeting probes capable of recognizing mixed-sequence dsDNA targets. However, they too require non-physiological salinity for optimal strand invasion.<sup>12</sup> In summary, oligonucleotide-based probes that recognize mixed-sequence dsDNA targets at physiologic conditions remain largely elusive.

We have recently introduced *Invaders* as an alternative strategy toward mixed-sequence dsDNA recognition.<sup>13</sup> These double-stranded probes are activated for dsDNA recognition through modification with +1 interstrand zippers of intercalator-functionalized nucleotides (for an illustration, see Figure 1; for a formal definition of the zipper nomenclature, see the Experimental section). This structural motif results in a locally perturbed and destabilized region

in the probe duplex since the motif represents a violation of the ‘nearest neighbor exclusion principle’, which states that intercalators, at most, bind to every second base pair of a DNA duplex due to limitations in local helix expandability.<sup>14</sup> On the other hand, the two strands comprising an Invader probe display exceptionally strong affinity toward complementary single-stranded DNA (cDNA), since duplex formation results in strongly stabilizing pyrene-nucleobase stacking interactions (Figure 1). In an important proof-of-concept study, we harnessed the energy difference between reactants (i.e., Invader probes and target duplexes) and products (i.e., probe-target duplexes) to drive recognition of chromosomal *DYZ-1* satellite DNA in male bovine kidney cells at non-denaturing conditions.<sup>13</sup>

We originally used 2'-*N*-(pyren-1-yl)methyl-2'-amino- $\alpha$ -L-LNA (Locked Nucleic Acid) nucleotides as the key activating components of Invader probes,<sup>15</sup> but recently discovered that they can be replaced by 2'-*O*-(pyren-1-yl)methyl-ribonucleotides (Figure 1).<sup>16</sup> The resulting probes display similar dsDNA-recognition efficiency and are much easier to synthesize.<sup>17,18</sup> Identification of these simple building blocks allowed us to initiate systematic structure-property relationship studies with the goal of gaining additional insights into the structural determinants governing Invader recognition efficiency. For example, we demonstrated that all four canonical 2'-*O*-(pyren-1-yl)methyl-RNA monomers can be used to construct dsDNA-binding Invader probes. However, probes using the pyrimidine monomers are particularly efficient.<sup>19</sup>

In the present study, we wanted to determine if the relative orientation between the pyrene intercalator and sugar skeleton has any impact on Invader-mediated recognition of mixed-sequence dsDNA. Toward this end, the corresponding 2- and 4-pyrenyl functionalized uridines were synthesized and incorporated into oligodeoxyribonucleotides (ONs), which were then characterized with respect to thermal denaturation, thermodynamic, UV-Vis absorption and

fluorescence properties (Figure 1). This was then followed by biophysical characterization of double-stranded probes with different interstrand arrangements of these monomers and recognition experiments using DNA hairpins as model targets.

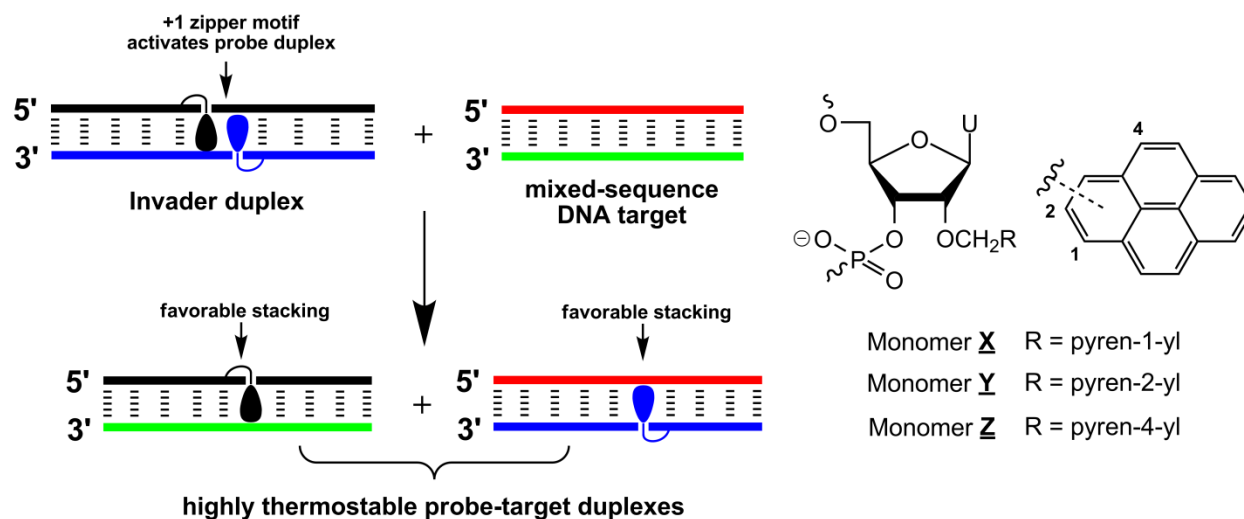
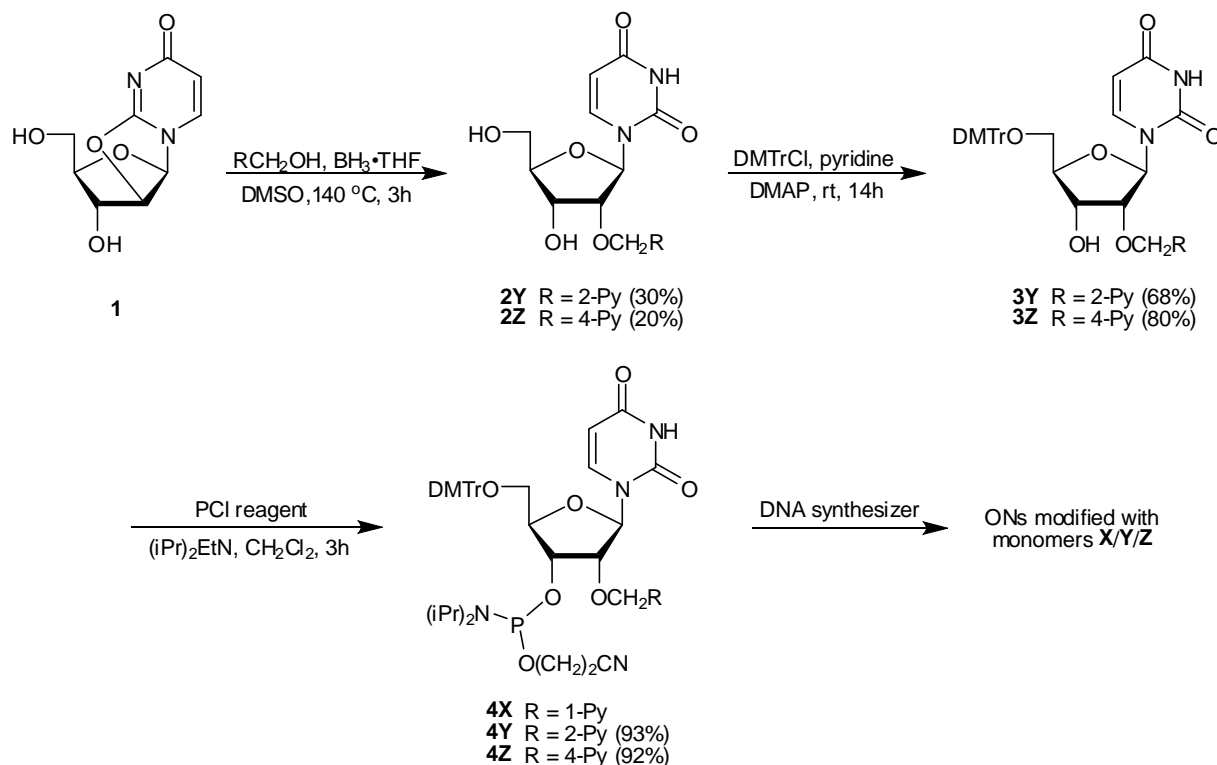


**Figure 1.** Illustration of the Invader approach for recognition of mixed-sequence DNA and structures of monomers used herein. Droplets denote pyrene moieties.

## RESULTS AND DISCUSSION

*Synthesis of O2'-pyrene-functionalized uridine phosphoramidites.* Phosphoramidites **4Y** and **4Z** were prepared in a similar manner as the 2'-O-(pyren-1-yl)methyl-uridine analogue **4X**.<sup>17b</sup> Thus, treatment of O2,O2'-anhydrouridine **1**<sup>20</sup> with tris(pyren-2-yl)methyl borate or tris(pyren-4-yl)methyl borate - generated in situ<sup>21</sup> via addition of 2-pyrenemethanol<sup>22</sup> or 4-pyrenemethanol<sup>23</sup> to borane - afforded **2Y** and **2Z** in modest but acceptable yields (30% and 20% respectively, Scheme 1). Subsequent O5'-dimethoxytritylation gave nucleosides **3Y** and **3Z**, which upon

treatment with 2-cyanoethyl-*N,N*-diisopropylchlorophosphoramidite (PCI reagent) and Hünig's base provided target phosphoramidites **4Y** and **4Z** in excellent yield.



**Scheme 1.** Synthesis of O2'-pyrene-functionalized uridine phosphoramidites **4Y** and **4Z**. DMTr = 4,4'-dimethoxytrityl; PCI reagent = 2-cyanoethyl-*N,N'*-diisopropylchlorophosphoramidite; 1-Py = pyren-1-yl; 2-Py = pyren-2-yl; 4-Py = pyren-4-yl.

*Synthesis of modified ONs and experimental design.* Phosphoramidites **4X**, **4Y** and **4Z** were used in machine-assisted solid-phase DNA synthesis to incorporate monomers **X-Z** into ONs using 4,5-dicyanoimidazole as an activator and extended hand-coupling (15 min), which resulted in stepwise coupling yields of ~99%/~99%/~98% for **4X/4Y/4Z**, respectively. The identity and purity of the modified ONs was established via MALDI-TOF (Table S1 in the ESI<sup>†</sup>) and ion-pair reverse phase HPLC (>85% purity), respectively.

Monomers **X-Z** were studied in 9-mer sequence contexts, which we have previously used to screen and identify potential Invader building blocks.<sup>16</sup> ONs containing a single incorporation in the 5'-GBG ATA TGC context are denoted **X1**, **Y1**, and **Z1**. Similar conventions apply for the **B2-B6** series (Table 1). Reference DNA and RNA strands are denoted **D1/D4** and **R1/R4**, respectively (see footnote, Table 1).

*Thermostability of duplexes with complementary DNA/RNA.* First, the thermostabilities of duplexes between **B1-B6** and complementary DNA or RNA targets were determined from thermal denaturation experiments performed in medium salt phosphate buffer ( $[\text{Na}^+] = 110 \text{ mM}$ , pH 7.0). The resulting denaturation curves display the expected monophasic sigmoidal transitions (Figure S1 in the ESI<sup>†</sup>). Interestingly, **Y**-modified ONs form much more thermostable duplexes with cDNA than unmodified ONs ( $\Delta T_m/\text{mod} = +6.0$  to  $+14.0 \text{ }^\circ\text{C}$ , Table 1). In fact, the resulting duplexes are even more thermostable than **X**-modified duplexes, suggesting that the 2-pyrenyl moiety of monomer **Y** is very well accommodated in DNA duplexes. In contrast, **Z**-modified ONs display considerably lower affinity toward cDNA ( $\Delta T_m/\text{mod} = -3.0$  to  $+9.0 \text{ }^\circ\text{C}$ , Table 1). The thermostability trends are sequence-dependent. Thus, ONs in which the pyrene-functionalized monomers are flanked by 3'-purines, induce greater stabilization than ONs with 3'-flanking pyrimidines (e.g., compare  $\Delta T_m/\text{mod}$  values for **B2**- and **B4**-series, Table 1). This is indicative of 3'-intercalative binding modes of the pyrene moieties,<sup>19,24</sup> as 3'-flanking purines would provide larger  $\pi$ -stacking surfaces than 3'-pyrimidines. Less stable duplexes are formed with cRNA ( $\Delta T_m/\text{mod} = -8.0$  to  $+7.5 \text{ }^\circ\text{C}$ , Table 1; trend: **Y** > **X** > **Z**), which also points to intercalative pyrene binding modes,<sup>18,24a,25</sup> as intercalators generally favor the less compressed *B*-type helix geometry of DNA:DNA duplexes.<sup>26</sup>



**Table 1.** Thermal denaturation temperatures ( $T_m$ 's) for duplexes between **B1-B6** and complementary DNA or RNA.<sup>a</sup>

ON	Sequence	B =	$T_m$ ( $\Delta T_m/\text{mod}$ ) [ $^{\circ}\text{C}$ ]					
			+ cDNA			+ cRNA		
			<b>X</b> <sup>b</sup>	<b>Y</b>	<b>Z</b>	<b>X</b> <sup>b</sup>	<b>Y</b>	<b>Z</b>
<b>B1</b>	5'- <b>GBG</b> ATA TGC		34.5 [+5.0]	35.5 [+6.0]	29.5 [±0.0]	24.5 [-2.0]	25.5 [-1.5]	20.5 [-6.0]
<b>B2</b>	5'-GTG <b>ABA</b> TGC		42.5 [+13.0]	43.5 [+14.0]	37.5 [+8.0]	30.5 [+4.0]	34.0 [+7.5]	27.5 [+1.0]
<b>B3</b>	5'-GTG ATA <b>BGC</b>		37.5 [+8.0]	39.0 [+9.5]	33.5 [+4.0]	26.5 [±0.0]	28.0 [+1.5]	21.5 [-5.0]
<b>B4</b>	3'-CAC <b>BAT</b> ACG		33.0 [+3.5]	35.5 [+6.0]	26.5 [-3.0]	20.5 [-4.5]	23.0 [-1.5]	16.5 [-8.0]
<b>B5</b>	3'-CAC TAB <b>ACG</b>		42.5 [+13.0]	43.5 [+14.0]	38.5 [+9.0]	27.5 [+2.5]	32.0 [+7.5]	26.5 [+2.0]
<b>B6</b>	3'-CAC <b>BAB</b> ACG		43.5 [+7.0]	45.5 [+8.0]	32.5 [+1.5]	24.0 [-0.3]	28.5 [+2.0]	16.5 [-4.0]

<sup>a</sup>  $\Delta T_m$  = change in  $T_m$  relative to reference duplexes **D1:D4** ( $T_m \equiv 29.5$   $^{\circ}\text{C}$ ), **D1:R4** ( $T_m \equiv 26.5$   $^{\circ}\text{C}$ ) or **R1:D4** ( $T_m \equiv 24.5$   $^{\circ}\text{C}$ ), where **D1**: 5'-GTGATATGC, **D4**: 3'-CACTATACG, **R1**: 5'-GUGAUAUGC and **R4**: 3'-CACUAUACG;  $T_m$ 's are determined as the maximum of the first derivative of melting curves ( $A_{260}$  vs  $T$ ) recorded in medium salt buffer ( $[\text{Na}^+] = 110$  mM,  $[\text{Cl}^-] = 100$  mM, pH 7.0 ( $\text{NaH}_2\text{PO}_4/\text{Na}_2\text{HPO}_4$ )), using 1.0  $\mu\text{M}$  of each strand.  $T_m$ 's are averages of at least two measurements within 1.0  $^{\circ}\text{C}$ ; A = adenin-9-yl DNA monomer, C = cytosin-1-yl DNA monomer, G = guanin-9-yl DNA monomer, T = thymin-1-yl DNA monomer. For structures of monomers **X-Z** see Figure 1.

<sup>b</sup> From reference 17b.

*Binding specificity.* Next, the binding specificity of singly modified ONs (**B2**-series) was studied using DNA targets with mismatched nucleotides opposite of the pyrene-functionalized monomer (Table 2). **X2/Y2/Z2** discriminate mismatched DNA targets less efficiently than reference strand **D1**, especially when a mismatched T is opposite of the modification. This is in agreement with other studies in which reduced binding specificity of intercalator-modified ONs was observed.<sup>26</sup> Interestingly, the specificity trends mirror the affinity trends. Thus, **Y2** discriminates mismatched target more efficiently than **X2**, which, conversely, discriminates mismatched targets more efficiently than **Z2**. Additional specificity data are discussed in the Electronic Supplementary Information (Tables S3 and S4 in the ESI<sup>†</sup>).

**Table 2.** Discrimination of mismatched DNA targets by **X2/Y2/Z2** and reference strands.<sup>a</sup>

ON	Sequence	<b>B</b> =	DNA: 3'-CAC <b>T</b> <u><b>B</b></u> T ACG			
			$T_m$ [°C]		$\Delta T_m$ [°C]	
			A	C	G	T
<b>D1</b>	5'-GTG ATA TGC		<b>29.5</b>	-16.5	-9.5	-17.0
<b>X2<sup>b</sup></b>	5'-GTG A <u>X</u> A TGC		<b>42.5</b>	-13.5	-5.5	-7.0
<b>Y2</b>	5'-GTG A <u>Y</u> A TGC		<b>43.5</b>	-16.5	-6.5	-9.0
<b>Z2</b>	5'-GTG A <u>Z</u> A TGC		<b>37.5</b>	-10.0	-4.0	-3.0

<sup>a</sup> For conditions of thermal denaturation experiments, see Table 1.  $T_m$ 's of fully matched duplexes are shown in bold.  $\Delta T_m$  = change in  $T_m$  relative to fully matched duplex.

<sup>b</sup> From reference 17b

*Optical spectroscopy.* UV-Vis absorption and steady-state fluorescence emission spectra of **X/Y/Z**-modified ONs in the presence or absence of complementary DNA/RNA targets were recorded next to further ascertain intercalative binding modes of the pyrene moieties, as intercalation is known to induce bathochromic shifts of pyrene absorption peaks<sup>27</sup> and nucleobase-mediated quenching of pyrene fluorescence.<sup>27a,28</sup> Indeed, **X/Y/Z**-modified ONs

generally display hypochromic and bathochromic shifts in the pyrene absorption spectra upon hybridization with DNA and RNA targets ( $\Delta\lambda_{\max} = 0\text{-}5$  nm, Table 3; Figures S2-S4 in the ESI<sup>†</sup>). Slightly greater bathochromic shifts are generally observed upon hybridization with DNA than RNA targets, which again may reflect the preference of intercalators for the less compressed geometry of *B*-DNA.

**Table 3.** Absorption maxima in the 335-355 nm region for single-stranded **X/Y/Z**-modified ONs and the corresponding duplexes with complementary DNA or RNA.<sup>a</sup>

ON	Sequence	$\lambda_{\max} [\Delta\lambda_{\max}] / \text{nm}$								
		<b>B</b> =	<b>X</b> <sup>b</sup>			<b>Y</b>			<b>Z</b>	
		SSP	+cDNA	+cRNA	SSP	+cDNA	+cRNA	SSP	+cDNA	+cRNA
<b>B1</b>	5'-G <u>B</u> G ATA TGC	350	353[+3]	352[+2]	344	346[+2]	345[+1]	343	344[+1]	343[±0]
<b>B2</b>	5'-GTG A <u>B</u> A TGC	348	353[+5]	352[+4]	342	345[+3]	345[+3]	340	343[+3]	343[+3]
<b>B3</b>	5'-GTG ATA <u>B</u> GC	350	353[+3]	352[+2]	344	346[+2]	345[+1]	343	344[+1]	343[±0]
<b>B4</b>	3'-CAC <u>B</u> AT ACG	350	352[+2]	352[+2]	344	345[+1]	345[+1]	342	344[+2]	343[+1]
<b>B5</b>	3'-CAC T <u>A</u> B ACG	349	353[+4]	352[+3]	343	345[+2]	345[+2]	342	344[+2]	344[+2]

<sup>a</sup> Measurements were performed at 5 °C using a spectrophotometer and quartz optical cells with 1.0 cm path lengths. Buffer conditions are as for thermal denaturation experiments.

<sup>b</sup> From reference 17b.

Steady-state fluorescence emission spectra of **X/Y/Z**-modified ONs and the corresponding duplexes with cDNA/cRNA display two vibronic bands at  $\lambda_{\text{em}} = 382\pm 3$  nm and  $402\pm 3$  nm, respectively, as well as a small shoulder at ~420 nm. As anticipated, the fluorescence intensity typically decreases upon hybridization with DNA/RNA targets, with greater decreases typically being observed upon DNA binding (Figure 2; Figures S5-S7 in the ESI<sup>†</sup>). Interestingly, duplexes modified with monomer **Z** are noticeably less fluorescent than **X**- or **Y**-modified duplexes.

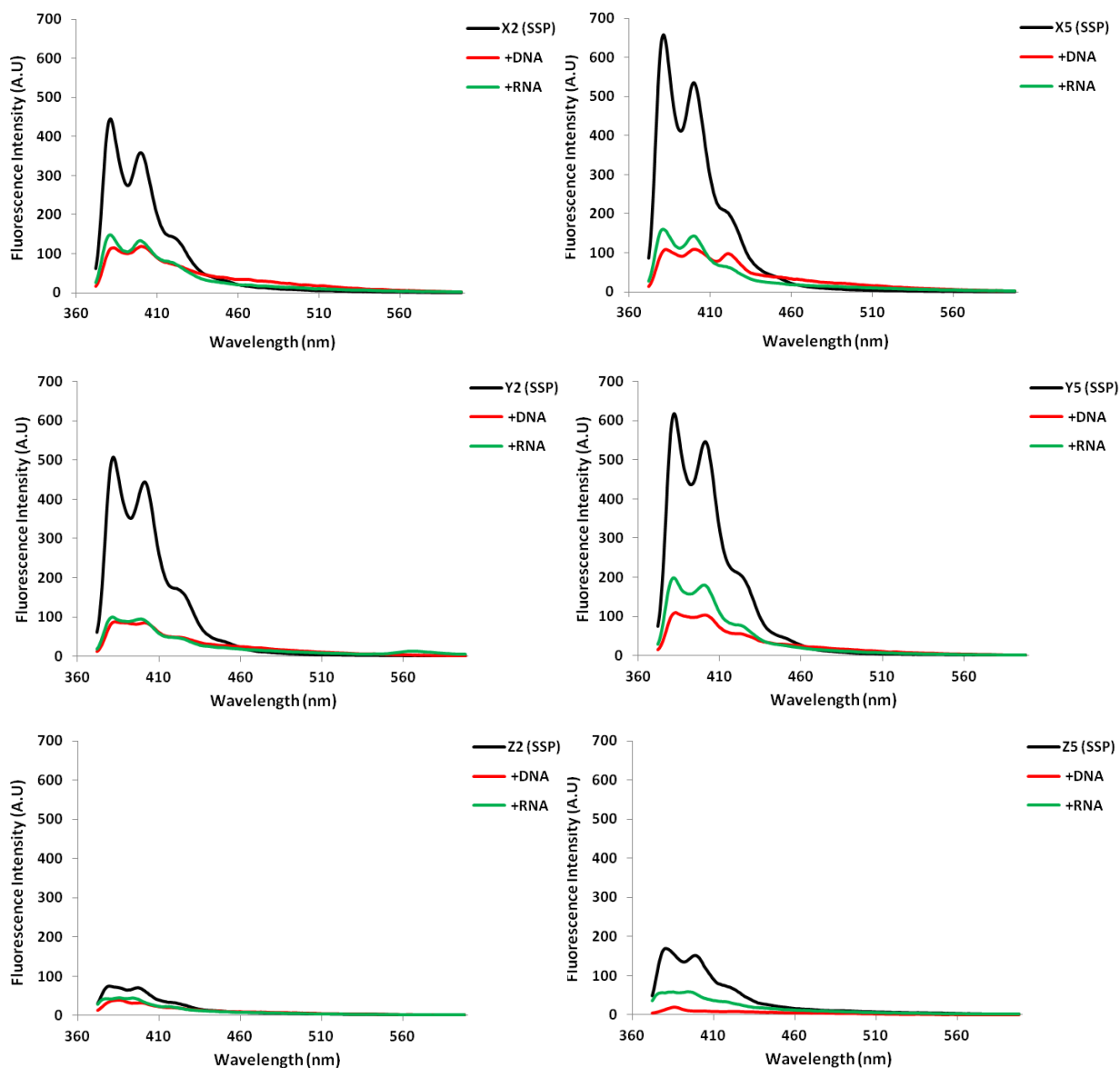


**Figure 2.** Steady-state fluorescence emission spectra of select **X/Y/Z**-modified ONs and corresponding duplexes with DNA/RNA targets. Spectra were recorded at  $T = 5\text{ }^{\circ}\text{C}$  using  $\lambda_{\text{ex}} = 350, 345$  and  $340\text{ nm}$  for **X**, **Y** and **Z**-modified ONs, respectively. Each strand was used at  $1.0\text{ }\mu\text{M}$  concentration in  $T_m$  buffer.

*Molecular modeling of probe-target duplexes.* To rationalize the observed biophysical trends, we performed force-field calculations on duplexes between **X2/Y2/Z2** and complementary DNA (residue numbering: 5'-G<sub>1</sub>T<sub>2</sub>G<sub>3</sub>A<sub>4</sub>B<sub>5</sub>A<sub>6</sub>T<sub>7</sub>G<sub>8</sub>C<sub>9</sub>:3'-C<sub>18</sub>A<sub>17</sub>C<sub>16</sub>T<sub>15</sub>A<sub>14</sub>T<sub>13</sub>A<sub>12</sub>C<sub>11</sub>G<sub>10</sub>). The complete data set of structural furanose, base pair and dinucleotide step parameters<sup>29</sup> is provided in the Electronic Supplementary Information (Tables S7-S8 and Figures S9-S14 in the ESI<sup>†</sup>).

In agreement with the photophysical data presented above, the pyrene moieties remain stably intercalated in the duplex core throughout the stochastic dynamics simulations (Figure 3 top - for details of calculation protocol, see Experimental section). Inspection of the structures reveals that the right-handed duplexes are elongated relative to the corresponding *B*-DNA reference duplex (e.g., *rise* increases from ~3.3 Å to ~7.3 Å across the B<sub>5</sub>A<sub>6</sub>:A<sub>14</sub>T<sub>13</sub> dinucleotide step, Figure S10 in the ESI<sup>†</sup>). The overlap between the pyrene and neighboring nucleobases is strongly influenced by the substitution pattern of the pyrene, which explains the observed thermostability trends ( $T_m$  decreases  $Y \geq X > Z$ ). The pyrene of monomer **X** stacks with the nucleobase moieties of X<sub>5</sub>, A<sub>6</sub> and A<sub>13</sub>, while the pyrene of monomer **Y** is positioned in a manner that facilitates stacking with all four neighboring nucleobase moieties (Figure 3 bottom). Conversely, the pyrene of monomer **Z** stacks only with the flanking nucleobases on its own strand, i.e., Z<sub>5</sub> and A<sub>6</sub>. The poorer fit of the pyrene of monomer **Z** is also reflected in greater perturbation across the B<sub>5</sub>A<sub>6</sub>:A<sub>14</sub>T<sub>13</sub> dinucleotide step, i.e., more pronounced *buckle* (~6° and ~ -4° in **D1:D4**, ~13° and ~ -10° in **X2:D4**, ~15° and ~ -11° in **Y2:D4**, and ~21° and ~ -19° in **Z2:D4**, Figure S9 in the ESI<sup>†</sup>) and decreased *roll* (~12° in **D1:D4**, ~ -10° in **X2:D4**, ~ -11° in **Y2:D4**, and ~ -19° in **Z2:D4**, Figure S10 in the ESI<sup>†</sup>). Another noteworthy observation is that the furanose rings of nucleotides X<sub>5</sub>A<sub>6</sub>, Y<sub>5</sub>A<sub>6</sub> and Z<sub>5</sub>A<sub>6</sub> generally exhibit increased *South* type character relative to the reference duplex ( $P = 124-171^\circ$  vs  $102-129^\circ$ ), presumably as a

consequence of  $\pi$ - $\pi$ -stacking between the pyrene and flanking nucleobases (Table S7 in the ESI<sup>†</sup>).

To sum up, the molecular modeling structures are useful in explaining the observed thermostability trends and photophysical properties of X/Y/Z-modified duplexes.

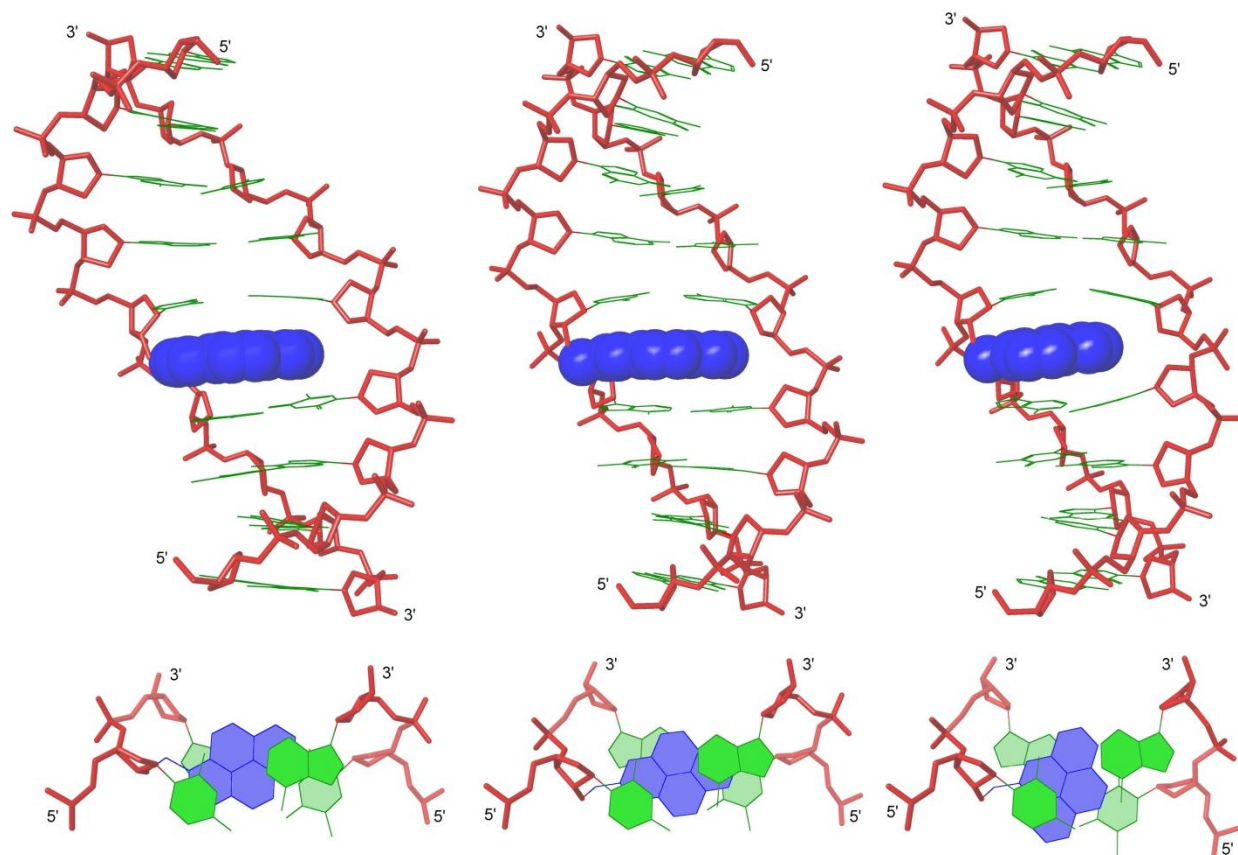


**Figure 3.** Lowest energy structures of X2:D4 (left), Y2:D4 (middle) and Z2:D4 (right). Upper: side view of duplex; lower: top view of the central duplex region. Color code: sugar phosphate backbone (red); pyrene moieties (blue) and nucleobases (green). Hydrogen atoms, sodium ions and bond orders are omitted for clarity.

*Biophysical properties of duplexes with interstrand zippers of X/Y/Z-monomers.* Next, we determined the thermostability of DNA duplexes with different interstrand zipper arrangements of **X/Y/Z** monomers to identify monomers and probe architectures that show the greatest potential for dsDNA-recognition. The impact on duplex thermostability upon incorporation of a second monomer can be additive, greater-than-additive or less-than-additive relative to the corresponding singly modified duplex. The impact is conveniently approximated in terms of  $T_m$ 's by the term 'deviation from additivity' ( $DA$ ) defined as:  $DA_{\mathbf{ON}_A:\mathbf{ON}_B} \equiv \Delta T_m(\mathbf{ON}_A:\mathbf{ON}_B) - [\Delta T_m(\mathbf{ON}_A:\text{cDNA}) + \Delta T_m(\text{cDNA}:\mathbf{ON}_B)]$ , where  $\mathbf{ON}_A:\mathbf{ON}_B$  is a duplex with an interstrand arrangement of monomers.  $DA$  also serves as an indicator for dsDNA-recognition potential. Probes with strongly negative  $DA$  values are likely to be activated for recognition of iso-sequential dsDNA via the process depicted in Figure 1, since the products of the recognition process (i.e., probe-target duplexes) are more thermostable than the reactants (i.e., probe duplexes and target duplexes). A more rigorous approach based on differences in  $\Delta G$  values of probe-target and Invader duplexes is discussed shortly.

As expected,<sup>13,15,16</sup> duplexes with +1 interstrand monomer arrangements are less thermostable and more strongly activated for dsDNA-recognition than duplexes with other arrangements (compare  $T_m$ 's and  $DA$  values for **B2:B5** relative to other probe duplexes, Table 4). Clearly the two pyrene-functionalized monomers interact with each other in an energetically unfavorable manner when placed in this motif. Interestingly, there is little difference in the dsDNA-targeting potential of **X2:X5**, **Y2:Y5** and **Z2:Z5** as judged by the  $DA$  values; the lower thermostability of **Z**-modified probe-target duplexes is compensated by an equivalent destabilization of the probe duplexes (compare  $DA$  values for **X2:X5**, **Y2:Y5** and **Z2:Z5**, Table 4).

The above  $T_m$ -based conclusions were corroborated through analysis of thermodynamic parameters for duplex formation, which were derived through fitting of thermal denaturation curves.<sup>30</sup> Thus, formation of probe-target duplexes is highly favorable relative to unmodified duplexes, with **Y**-modified and **Z**-modified ONs leading to the most and least stable duplexes with cDNA, respectively (see the first two  $\Delta\Delta G^{293}$  columns, Table 4). Stabilization of the probe-target duplexes is largely a consequence of increased entropy (Tables S5 and S6 in the ESI<sup>†</sup>). On the other hand, **B2:B5** duplexes are much less stable (see the third  $\Delta\Delta G^{293}$  column, Table 4) due to strongly increased enthalpy (Tables S5 and S6 in the ESI<sup>†</sup>). Consequentially, **B2:B5** probes display favorable binding free energy for recognition of iso-sequential dsDNA targets as given by  $\Delta G_{rec}^{293}(\text{ON}_A:\text{ON}_B) = \Delta G^{293}(\text{ON}_A:\text{cDNA}) + \Delta G^{293}(\text{cDNA}:\text{ON}_B) - \Delta G^{293}(\text{ON}_A:\text{ON}_B) - \Delta G^{293}(\text{dsDNA})$  (i.e.,  $\Delta G_{rec}^{293}$  for **B2:B5**  $\ll 0$  kJ/mol, Table 4). **X2:X5** and **Y2:Y5** display very similar  $\Delta G_{rec}^{293}$  values. Unfortunately, the absence of a clear lower base line in the thermal denaturation curve of **Z2:Z5** precluded determination of  $\Delta G_{rec}^{293}$  for this duplex. Probes with other interstrand arrangements of **X/Y/Z**-monomers are much more stable and display much less favorable binding free energy for recognition of iso-sequential dsDNA targets ( $\Delta G_{rec}^{293}$  between -8 and 0 kJ/mol, Table 4), presumably since the two monomers act independently from each other.



Table 4. Properties of X/Y/Z-modified probe duplexes.<sup>a</sup>

ON	ZP	Sequence	$T_m$ (°C)	$DA$ (°C)	$\Delta G^{293}[\Delta\Delta G^{293}]$ (kJ/mol)			$\Delta G_{rec}^{293}$ (kJ/mol)	$\lambda_{max}$ (nm)
					upper ON vs cDNA	lower ON vs cDNA	Probe duplex		
X1 X5	+4	5'-G <u>X</u> G ATA TGC 3'-CAC TAX <u>X</u> ACG	47.5	±0.0	-46±0 [-5]	-52±0 [-11]	-55±1 [-14]	-2	352
X1 X4	+2	5'-G <u>X</u> G ATA TGC 3'-CAC <u>X</u> AT ACG	31.5	-6.5	-46±0 [-5]	-46±0 [-5]	-45±1 [-4]	-6	350
X2 X5	+1	5'-GTG A <u>X</u> A TGC 3'-CAC TAX <u>X</u> ACG	<b>26.5</b>	<b>-29.0</b>	<b>-55±1 [-14]</b>	<b>-53±1 [-12]</b>	<b>-38±1 [+3]</b>	<b>-29</b>	<b>348</b>
X2 X4	-1	5'-GTG A <u>X</u> A TGC 3'-CAC <u>X</u> AT ACG	39.5	-6.5	-54±0 [-13]	-46±0 [-5]	-51±1 [-10]	-8	351
X3 X5	-1	5'-GTG ATA <u>X</u> GC 3'-CAC TAX <u>X</u> ACG	45.5	-5.0	-50±0 [-9]	-52±0 [-11]	-55±1 [-14]	-6	352
X3 X4	-3	5'-GTG ATA <u>X</u> GC 3'-CAC <u>X</u> AT ACG	40.5	-0.5	-50±0 [-7]	-46±0 [-3]	-53±1 [-10]	±0	352
Y1 Y5	+4	5'-G <u>Y</u> G ATA TGC 3'-CAC TAY <u>Y</u> ACG	48.5	-1.0	-48±0 [-7]	-55±1 [-14]	-56±1 [-15]	-6	346
Y1 Y4	+2	5'-G <u>Y</u> G ATA TGC 3'-CAC <u>Y</u> AT ACG	35.5	-6.0	-48±0 [-7]	-46±0 [-5]	-45±1 [-4]	-8	346
Y2 Y5	+1	5'-GTG A <u>Y</u> A TGC 3'-CAC TAY <u>Y</u> ACG	<b>28.5</b>	<b>-29.5</b>	<b>-56±0 [-15]</b>	<b>-55±1 [-14]</b>	<b>-43±1 [-2]</b>	<b>-27</b>	<b>339</b>
Y2 Y4	-1	5'-GTG A <u>Y</u> A TGC 3'-CAC <u>Y</u> AT ACG	43.5	-6.0	-56±0 [-15]	-46±0 [-5]	-55±1 [-14]	-6	346
Y3 Y5	-1	5'-GTG ATA <u>Y</u> GC 3'-CAC TAY <u>Y</u> ACG	47.5	-5.5	-51±1 [-10]	-55±1 [-14]	-58±1 [-17]	-7	346
Y3 Y4	-3	5'-GTG ATA <u>Y</u> GC 3'-CAC <u>Y</u> AT ACG	43.0	-2.0	-51±1 [-10]	-46±0 [-5]	-53±1 [-12]	-3	346
Z1 Z5	+4	5'-G <u>Z</u> G ATA TGC 3'-CAC TAZ <u>Z</u> ACG	38.5	±0.0	-44±0 [-3]	-48±1 [-7]	-49±1 [-8]	-2	345
Z1 Z4	+2	5'-G <u>Z</u> G ATA TGC 3'-CAC <u>Z</u> AT ACG	27.5	+1.0	-44±0 [-3]	-41±0 [±0]	-41±1 [±0]	-3	342
Z2 Z5	+1	5'-GTG A <u>Z</u> A TGC 3'-CAC TAZ <u>Z</u> ACG	<b>19.5</b>	<b>-27.0</b>	<b>-48±1 [-7]</b>	<b>-48±1 [-7]</b>	<b>N/A</b>	<b>N/A</b>	<b>339</b>
Z2 Z4	-1	5'-GTG A <u>Z</u> A TGC 3'-CAC <u>Z</u> AT ACG	30.5	-4.0	-48±1 [-7]	-41±0 [±0]	-41±1 [±0]	-7	344
Z3 Z5	-1	5'-GTG ATA <u>Z</u> GC 3'-CAC TAZ <u>Z</u> ACG	37.0	-5.5	-46±0 [-5]	-48±1 [-7]	-46±1 [-5]	-7	345
Z3 Z4	-3	5'-GTG ATA <u>Z</u> GC 3'-CAC <u>Z</u> AT ACG	32.5	+2.0	-46±0 [-5]	-41±0 [±0]	-42±1 [-1]	-4	345

<sup>a</sup> ZP = zipper. For conditions of thermal denaturation and absorption experiments, see Table 1 and Table 3, respectively.  $DA = \Delta T_m$  (Invader) - ( $\Delta T_m$  (upper strand vs cDNA) +  $\Delta T_m$  (lower strand vs cDNA)).  $\Delta\Delta G^{293}$  is measured relative to  $\Delta G^{293}$  for **D1:D4** = -41 kJ/mol.  $\Delta G_{rec}^{293} = \Delta G^{293}$  (upper strand vs cDNA) +  $\Delta G^{293}$  (lower strand vs cDNA) -  $\Delta G^{293}$  (probe duplex) -  $\Delta G^{293}$  (dsDNA target). "±" denotes standard deviation. N/A = the absence of a clear lower base line prevented determination of this value.  $T_m$ 's for X-modified duplexes have been previously published in reference 17b but are included to facilitate direct comparison.

The unique characteristics of duplexes with +1 interstrand monomer arrangements relative to other probe duplexes are also reflected in the blue-shifted pyrene absorption peaks (Figure S8 in the ESI<sup>†</sup>), which are indicative of reduced pyrene-nucleobase interactions (compare  $\lambda_{\text{max}}$  for **B2:B5** with  $\lambda_{\text{max}}$  for other probe duplexes (Table 4) or probe-target duplexes (Table 3)).

All probe duplexes exhibit vibronic peaks at  $\lambda_{\text{em}} = 380 \pm 2$  nm,  $400 \pm 3$  nm and  $\sim 420 \pm 3$  nm in their steady-state fluorescence emission spectrum (Figure 4). In addition, duplexes with +2 interstrand monomer arrangements display prominent and unstructured emission centered at  $\lambda_{\text{em}} \sim 490$  nm, which is consistent with pyrene excimer emission (Figure 4).<sup>15,16,19,31</sup> The presence of these signals shows that the pyrene moieties are stacking with an interplanar separation of  $\sim 3.4$  Å. We speculate that stacking occurs in the major groove in a similar manner as previously suggested for duplexes with +2 zipper arrangements of pyrene-functionalized *ara*-uridine monomers.<sup>31b,32</sup> Duplexes with +1 interstrand monomer arrangements also display excimer emission albeit of much weaker intensity. In this case, the two pyrene moieties most likely stack inside the duplex core in a similar manner as recently suggested for duplexes modified with 2'-*N*-(pyren-1-yl)methyl-2'-amino- $\alpha$ -L-LNA monomers; the spatial separation for pyrene-pyrene stacking in the major groove is too large.<sup>15a,16</sup> Dual intercalation would also explain the energetic lability of the **B2:B5** duplexes, as a localized region with one intercalator per base pair would ensue, which represents a violation of the 'nearest neighbor exclusion principle'.<sup>14</sup>

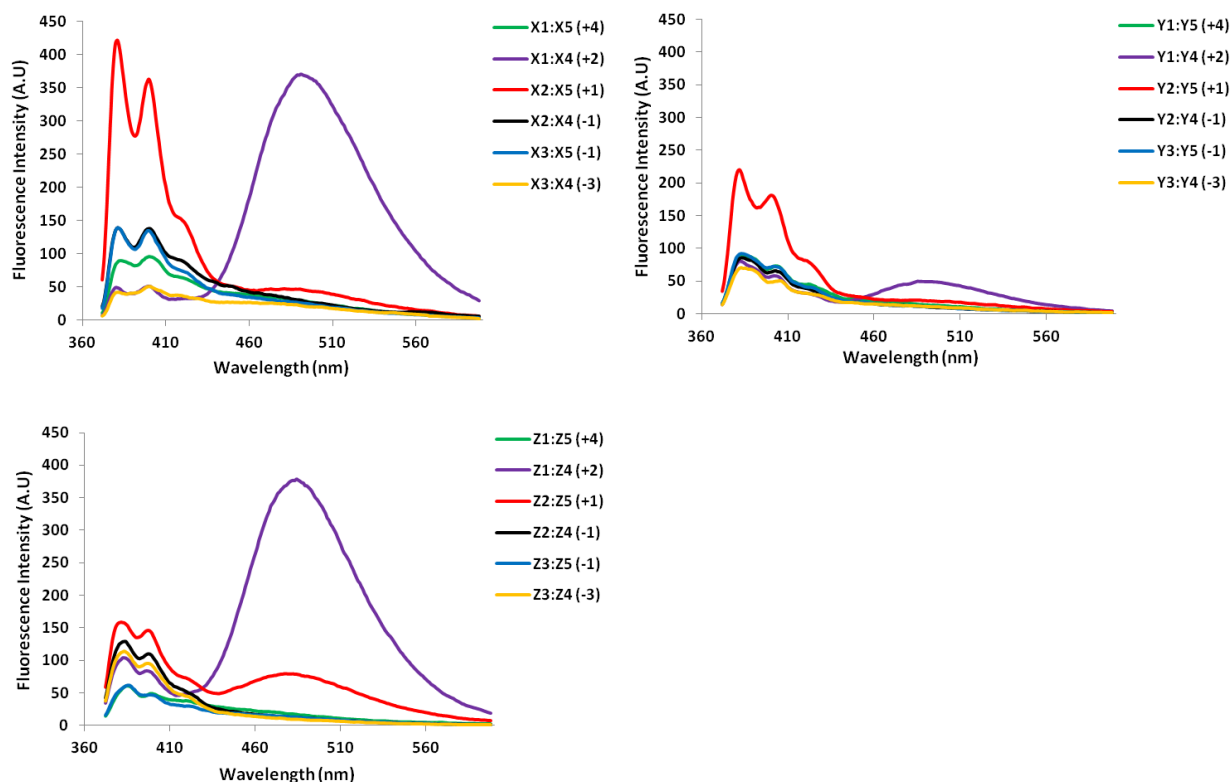


**Figure 4.** Steady-state fluorescence emission spectra of duplexes with different interstrand monomer arrangements of **X**, **Y**, and **Z** (zipper type indicated in parenthesis). For experimental conditions, see Figure 2. Spectra for **X**-modified duplexes were previously reported in reference 16 but are included for comparison.

*Molecular modeling of B2:B5 duplexes.* Force-field based simulations of **B2:B5** duplexes were performed to gain additional insight into the binding mode of the pyrene moieties. The results of these simulations point toward two possible binding modes, i.e., Type A in which both pyrene moieties intercalate into the duplex core (Figure 5) and Type B in which one pyrene is intercalating and the other is extruded into the major groove (Figure S15 in the ESI<sup>†</sup>). The presence of excimer signals in the steady state emission spectra of **X2:X5** and **Z2:Z5** (Figure 4), suggests that these duplexes are capable of adopting Type A conformations. However, the weak

intensity of the excimer signals – especially with **Y2:Y5** – suggests that **B2:B5** duplexes equilibrate between Type A and Type B conformations. Type A structures are characterized by significant elongation (*rise*  $\sim 10\text{\AA}$ ) and local perturbation (*buckle*  $\sim 30^\circ$  and  $\sim -30^\circ$  at  $B_5A_6$  and  $A_{14}B_{13}$ , respectively, and *roll*  $\sim -30^\circ$  across  $X_5A_6:X_{14}B_{13}$  and  $Y_5A_6:Y_{14}B_{13}$  and  $\sim -18^\circ$  across  $Z_5A_6:A_{14}$ ) (Figures S11-S12 in the ESI<sup>†</sup>). Type B structures are less elongated (*rise*  $\sim 7.5\text{\AA}$ ) and less perturbed (*buckle*  $\sim 20^\circ$  and  $\sim -20^\circ$  at  $B_5A_6$  and  $A_{14}B_{13}$ , respectively, and *roll*  $\sim -5^\circ$ ) (Figures S13-S14 in the ESI<sup>†</sup>). Both conformations can account for the lability of the **B2:B5** duplexes; base pairing in the vicinity of the interstrand zipper is distorted in both structures and the presence of a large hydrophobic pyrene in the major groove (Type B) will almost certainly perturb the stabilizing hydration layer or cause unfavorable steric interactions.

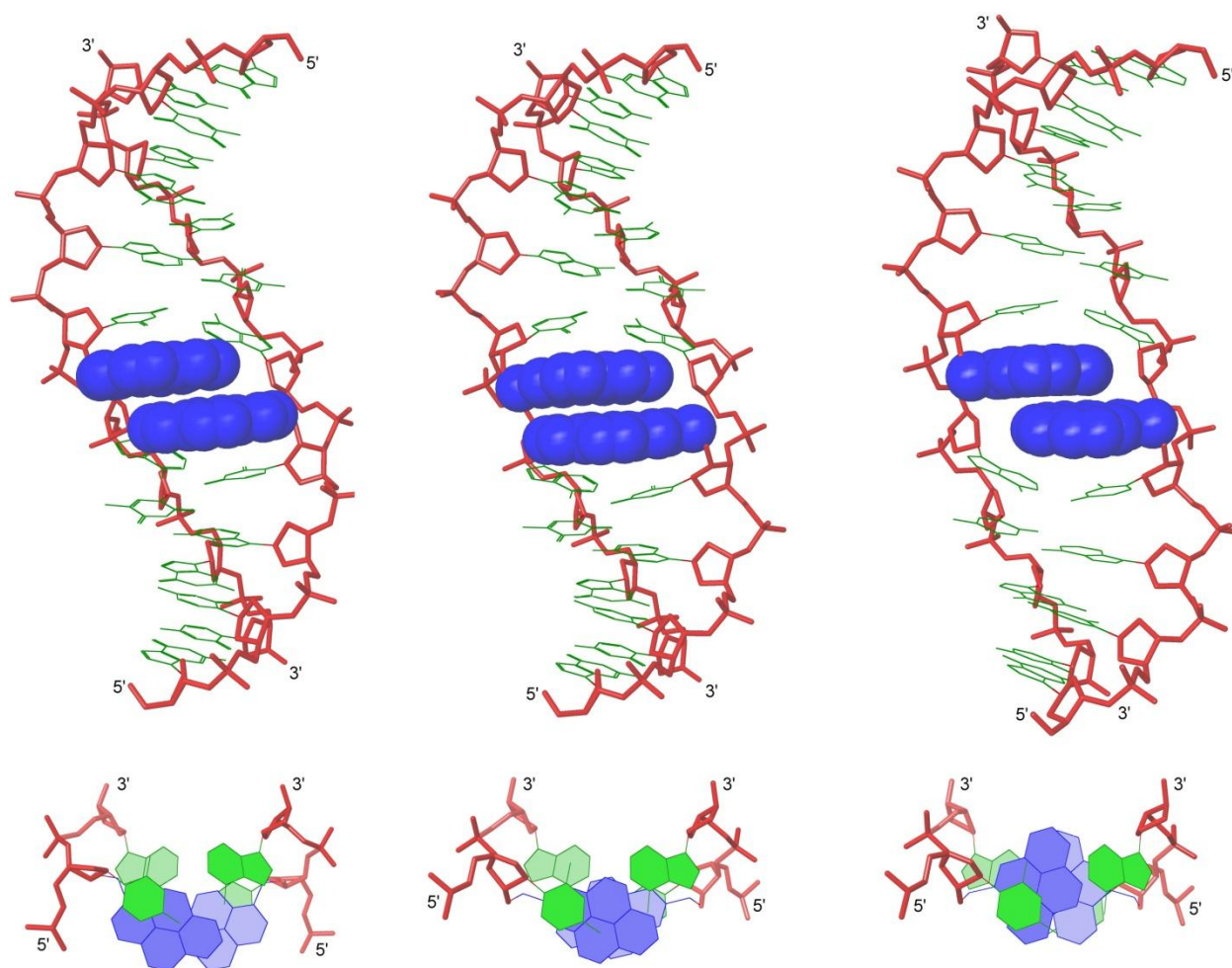


**Figure 5.** Lowest energy structures of X2:X5 (left), Y2:Y5 (middle) and Z2:Z5 (right) in Type A conformation. Top: side view of duplex; bottom: top view of the central duplex region. For color code, see Figure 3.

*Recognition of DNA hairpins using activated probe duplexes.* The  $\Delta G_{rec}^{293}$  values indicate that duplexes with +1 interstrand zippers of **X/Y/Z** monomers are the most strongly activated probes for dsDNA-recognition (Table 4). We therefore decided to evaluate these probes in greater detail using a gel shift assay that we have used to screen other potential Invader monomers with.<sup>13,16</sup> Thus, a digoxigenin (DIG) labeled DNA hairpin (DH) – comprised of a 9-mer double-stranded mixed-sequence stem that is linked by a T<sub>10</sub> loop – was used as a model target (Figure 6a).<sup>33</sup> As expected, the unimolecular nature of **DH1** strongly stabilizes the stem region as seen from the significantly higher  $T_m$  relative to the corresponding linear DNA duplex ( $T_m = 57.0$  °C vs 29.5 °C, respectively; Figure 6b and Table 1). Incubation of **DH1** with **X2:X5** or **Y2:Y5** in a HEPES buffer for 15 h at ambient temperature resulted in dose-dependent recognition as evidenced by the emergence of a slower migrating band on non-denaturing PAGE gels (Figure 6c).<sup>33</sup> It is particularly noteworthy that as little as 1.0 molar equivalent of **Y2:Y5** resulted in ~50% dsDNA-recognition (Figure 6d). In contrast, very little recognition was observed even at 500-fold molar excess of **Z2:Z5** (Figure 6c and 6d). This was surprising to us considering the very similar  $DA$  values of the **B2:B5** duplexes (Table 4). To determine if the poor dsDNA-recognition efficiency of **Z2:Z5** was due to insufficient stability of the recognition complex and/or slow reaction kinetics, we performed separate experiments in which **DH1** was annealed in the presence of 500-fold molar excess of **X2:X5** or **Z2:Z5** (i.e., heated to 95 °C for 2 min, cooled to 8° over 3 h, then analyzed on non-denaturing PAGE gels). The resulting gel electrophoretograms (results not shown) were essentially identical to those from the room temperature incubation experiments discussed above, which suggests that the recognition complex between **Z2:Z5** and **DH1** is not sufficiently stable at the experimental conditions of the assay.

As expected, the unmodified control duplex **D1:D4** did not result in formation of recognition complexes even when used at 500-fold molar excess, as there is no driving force to overcome the energetic penalty of opening **DH1** (Figure 6c). The use of 500-fold molar excess of single-stranded **X2/X5/Y2/Y5** only resulted in 15-40% recognition of **DH1** (Figure 6e), which demonstrates that both probe strands are necessary for efficient dsDNA-recognition.

Finally, the binding specificity of **X2:X5** and **Y2:Y5** was examined in detail by incubating the probe duplexes with DNA hairpins **DH2-DH7**, which are fully base-paired but singly mismatched relative to the Invader probes (underlined residues indicate position of sequence deviation, Figure 6b). Importantly, neither a 500-fold molar excess of **X2:X5** nor **Y2:Y5** resulted in recognition of the singly mismatched DNA hairpins, which demonstrates that hairpin recognition is highly specific (Figure 6f).

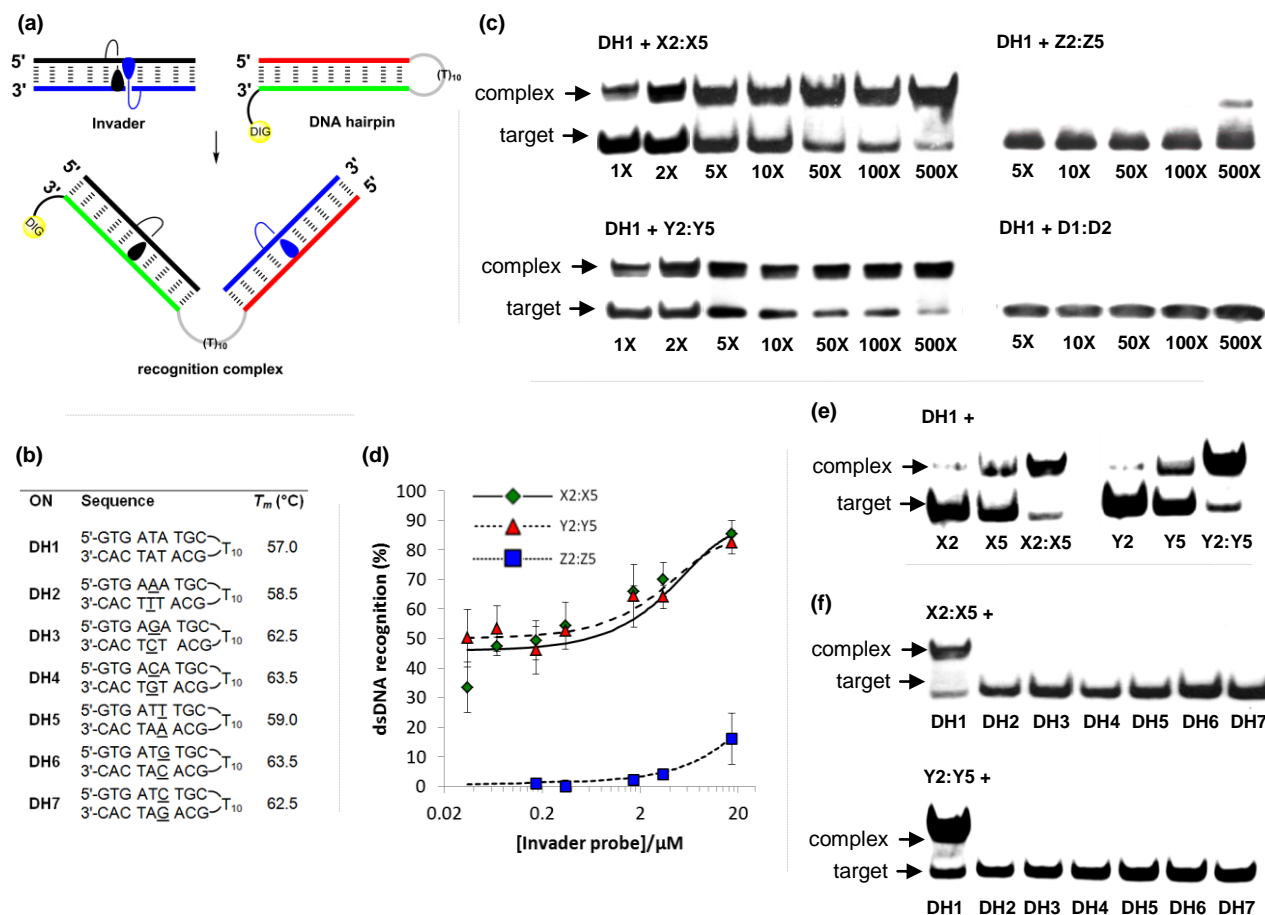


**Figure 6.** Recognition of model dsDNA targets using activated probe duplexes. (a) Illustration of recognition process; (b) sequences and intramolecular  $T_m$ 's of DNA hairpins with isosequential (DH1) or mismatched stems (DH2-DH7) relative to B2:B5 probes (for conditions of thermal denaturation experiments, see Table 1); (c) representative gel electrophoretograms illustrating recognition of DH1 using 1- to 500-fold molar excess of X2:X5, Y2:Y5, Z2:Z5, or unmodified D1:D4; (d) dose-response curves (average of three independent experiments; error bars represent standard deviation); (e) incubation of DH1 with 500-fold molar excess of single-stranded X2, X5, Y2 or Y5 or double-stranded X2:X5 or Y2:Y5; (f) gel electrophoretograms illustrating incubation of DH1-DH7 with 500-fold molar excess of X2:X5 or Y2:Y5. Experimental conditions for electrophoretic mobility shift assay: separately pre-annealed targets (34.4 nM) and probes (variable concentration) were incubated for 15 h at ambient temperature in 1X HEPES



buffer (50 mM HEPES, 100 mM NaCl, 5 mM MgCl<sub>2</sub>, 10% sucrose, 1.4 mM spermine tetrahydrochloride, pH 7.2) and then run on 16% non-denaturing PAGE (performed at 70V, 2 h, ~4 °C) using 0.5x TBE as a running buffer (45 mM Tris, 45 mM boric acid, 1 mM EDTA); DIG: digoxigenin.

**CONCLUSION.** Short synthetic routes to suitably protected 2'-*O*-(pyren-2-yl)-methyluridine and 2'-*O*-(pyren-4-yl)methyluridine have been developed. ONs modified with 2'-*O*-(pyren-2-yl)methyluridines display greater affinity toward complementary DNA and better mismatch discrimination than ONs modified with the corresponding 1-pyrenyl or 4-pyrenyl analogues. Molecular modeling suggests this to be a consequence of more efficient  $\pi$ - $\pi$ -stacking between the intercalating pyrene moiety and neighboring base pairs.

DNA duplexes with +1 interstrand arrangements of these pyrene-functionalized monomers display lower thermostability, more blue-shifted pyrene absorption maxima, more distinctive fluorescence emission profiles and greater potential for dsDNA-recognition than duplexes with other monomer arrangements. Force field simulations suggest that the +1 zipper motif results in significant perturbation of the duplex. Although the chemical differences between the three studied monomers are relatively minor, significant variations in the dsDNA-recognition efficiencies of the resulting probes are observed. Thus, probes with +1 interstrand zippers of 2'-*O*-(pyren-2-yl)methyluridines recognize mixed-sequence DNA hairpins very efficiently, whereas probes constructed with the corresponding 2'-*O*-(pyren-4-yl)methyluridines do not. Remarkably, Invaders based on 2'-*O*-(pyren-2-yl)methyluridines result in ~50% recognition of dsDNA when used in equimolar quantities. These findings encourage additional structure-property relationship studies based on the 2-pyrenyl scaffolds with the goal of further

increasing the dsDNA recognition efficiency of Invader probes, especially considering that detection of chromosomal DNA using Invaders based on the slightly less efficient 2'-*O*-(pyren-1-yl)-RNA monomers already has been demonstrated.<sup>13</sup> Proof-of-concept studies aiming at expanding the repertoire of applications for Invader probes in molecular biology, nucleic acid diagnostics and medicinal chemistry are ongoing and will be reported in due course.

## EXPERIMENTAL

**Preparation of 2-pyrenemethanol.** 2-Pyrenemethanol was obtained from 4,5,9,10-tetrahydropyrene by combining known literature protocols.<sup>22</sup> First, a solution of bromine (1.24 mL, 24.2 mmol) in anhydrous DMF (40 mL) was added dropwise over 2h to a room temperature solution of 4,5,9,10-tetrahydropyrene<sup>22a</sup> (5.00 g, 24.2 mmol) in anhydrous DMF (40 mL). The mixture was stirred for 4h at rt after completed addition, poured into cold water and stirred overnight. The resulting precipitate was filtered, washed with water, dried and purified by silica gel column chromatography (petroleum ether) to provide an off-white solid material (5.50 g), which was used in the next step without further purification.

The solid material was dissolved in anhydrous benzene (400 mL) along with DDQ (14.4 g, 63.6 mmol), and the solution was refluxed under an argon atmosphere for 4h. The resulting slurry was filtered through a pad of celite, which was thoroughly washed with benzene. The filtrate was washed with aq. NaOH (10% v/v, 3 x 100 mL) and water (3 x 100 mL). The organic phase was evaporated to dryness and the resulting residue purified by silica gel column chromatography (petroleum ether) to afford a pale yellow solid material (4.60 g), which was used in the next step without further purification.

Next, *n*-butyllithium (9.82 mL, 24.5 mmol, 2.5 M in hexane) was added slowly to a -78 °C solution of the solid material in anhydrous ether/THF (350 mL, 1:1 v/v). The brightly red solution was stirred at -78 °C for 2h and then slowly treated with anhydrous DMF (2.6 mL, 33.5 mmol). The reaction mixture was stirred at -30 to -50 °C for 1h and then at rt for an additional 15h. At this point, the reaction mixture was poured into ice-cold water (~100 mL) and the aqueous phase was extracted with EtOAc (3 x 100 mL). The combined organic layers were evaporated to near dryness and the resulting residue was purified by silica gel column chromatography (0-3% CH<sub>2</sub>Cl<sub>2</sub> in petroleum ether, v/v) to afford a brightly yellow solid material (3.50 g), which was used in the next step without further purification.

Lastly, sodium borohydride (0.69 g, 18.2 mmol) was added to a solution of this solid material in anhydrous THF (120 mL) and the reaction mixture was stirred overnight at rt. The reaction mixture was cooled on an ice bath and aqueous NaHCO<sub>3</sub> (10 % v/v, 50 mL) was added carefully. The aqueous layer was extracted with EtOAc (3 x 100 mL) and the combined organic layers were evaporated to dryness. The resulting residue was purified by silica gel column chromatography (0-1% MeOH in CH<sub>2</sub>Cl<sub>2</sub>, v/v) to afford 2-pyrenemethanol<sup>22c</sup> (3.45 g, 62% over four steps) as a white solid material. *R<sub>f</sub>* = 0.5 (10% MeOH in CH<sub>2</sub>Cl<sub>2</sub>, v/v); MALDI-HRMS *m/z* 232.0875 ([M]<sup>+</sup>, C<sub>17</sub>H<sub>12</sub>O, Calc. 232.0888); <sup>1</sup>H NMR (500 MHz, DMSO-*d*<sub>6</sub>): δ 8.28 (d, 2H, *J* = 7.8 Hz, H6/H8), 8.25 (s, 2H, H1/H3), 8.17 (s, 4H, H4/H5/H9/H10), 8.03-8.06 (ap t, 1H, *J* = 7.5 Hz, H7), 5.52 (t, 1H, ex, *J* = 5.7 Hz, OH), 4.97 (d, 2H, *J* = 5.7 Hz, CH<sub>2</sub>OH); <sup>13</sup>C NMR (DMSO-*d*<sub>6</sub>) δ 140.7 (C2), 130.5, 130.4, 127.31 (C4/C5),<sup>34</sup> 127.29 (C9/C10), 125.9 (C7), 124.9 (C6/C8), 123.8, 123.0 (C1/C3), 122.9, 63.2 (CH<sub>2</sub>Py).

**Preparation of 4-pyrenemethanol.** 4-Pyrenemethanol was obtained from 4,5,9,10-tetrahydropyrene by combining known literature protocols<sup>23</sup> and protocols for the synthesis of 2-pyrenemethanol. First, a solution of bromine (0.62 mL, 12.0 mmol) in glacial acetic acid (25 mL) was added dropwise over 1h to a room temperature solution of 4,5,9,10-tetrahydropyrene **3**<sup>22a</sup> (2.50 g, 12.0 mmol) in glacial acetic acid (25 mL). After ended addition, the reaction mixture was heated to 80 °C for 30 min, and then slowly cooled to rt, leading to the formation of a precipitate, which was isolated to provide a white solid material (2.90 g, 10.1 mmol) which used in the next step without further purification.

The solid material and DDQ (7.56 g, 33.3 mmol) were dissolved in anhydrous benzene (300 mL) and refluxed for 4h. The resulting slurry was filtered through a celite pad, which was thoroughly washed with benzene. The filtrate was washed with aq. NaOH (10% v/v, 3 x 80 mL) and water (3 x 80 mL). The organic phase was evaporated to dryness and the resulting residue purified via silica gel column chromatography (petroleum ether) to obtain a pale yellow solid (2.00 g), which was used in the next step without further purification.

Next, *n*-butyllithium (4.27 mL, 10.7 mmol, 2.5 M in hexane) was added slowly to a -78 °C solution of this solid material in anhydrous ether/THF (170 mL, 1:1 v/v). The brightly red solution was stirred at -78 °C for 2h and then treated slowly with anhydrous DMF (1.12 mL, 14.6 mmol). The reaction mixture was stirred at -30 to -50 °C for 1h and then at rt for additional 15h. The reaction mixture was poured into ice-cold water (~50 mL), the aqueous phase was extracted with EtOAc (3 x 50 mL), and the combined organic phase evaporated to dryness. The resulting residue was purified by silica gel column chromatography (0-3% CH<sub>2</sub>Cl<sub>2</sub> in pet ether, v/v) to afford a brightly yellow solid material (1.20 g), which was used in the next step without further purification.

Finally, NaBH<sub>4</sub> (0.24 g, 6.25 mmol) was added to a solution of the solid material in anhydrous THF (80 mL) and the reaction mixture was stirred overnight at rt. The reaction mixture was cooled on an ice-bath and aqueous NaHCO<sub>3</sub> (10 % v/v, 20 mL) was added carefully. The aqueous layer was extracted with EtOAc (3 x 80 mL) and the combined organic layers were evaporated to dryness. The resulting residue was purified by silica gel column chromatography (0-1% MeOH in CH<sub>2</sub>Cl<sub>2</sub>, v/v) to afford 4-pyrenemethanol (1.15 g, 41% over four steps) as a white solid material. *R<sub>f</sub>* = 0.5 (10% MeOH in CH<sub>2</sub>Cl<sub>2</sub>, v/v); MALDI-HRMS *m/z* 232.0881 ([M]<sup>+</sup>, C<sub>17</sub>H<sub>12</sub>O, Calc. 232.0888); <sup>1</sup>H NMR (DMSO-*d*<sub>6</sub>): δ 8.39-8.41 (dd, 1H, *J* = 7.4 Hz, 0.8 Hz, H3), 8.26-8.32 (m, 3H, H1/H6/H8), 8.24 (s, 1H, H5), 8.17-8.21 (2d, 2H, *J* = 8.8 Hz, H9/H10), 8.05-8.11 (m, 2H, H2/H7), 5.53 (t, 1H, ex, *J* = 5.5 Hz, OH), 5.19-5.21 (dd, 2H, *J* = 5.5 Hz, 0.8 Hz, CH<sub>2</sub>Py); <sup>13</sup>C NMR (DMSO-*d*<sub>6</sub>) δ 137.1, 130.9, 130.4, 130.3, 128.9, 127.4 (C9/C10), 127.1 (C9/C10), 126.2 (C2/C7), 125.9 (C2/C7), 125.1 (C1/C6/C8), 125.0 (C1/C6/C8), 124.8 (C1/C6/C8), 124.3 (C5), 124.0, 123.2, 121.2 (C3), 61.4 (CH<sub>2</sub>Py).

**General O2'-alkylation protocol for the preparation of 2Y/2Z (description for ~4.4mmol scale).** The appropriate pyrenemethanol, solid NaHCO<sub>3</sub> and borane (1.0 M solution in THF) were placed in a pressure tube, suspended in anhydrous DMSO and stirred under an argon atmosphere at rt until effervescence ceased (~10 min). At this point, O2,O2'-anhydrouridine **1**<sup>20</sup> was added (specific quantities of substrates and reagents are given below), the pressure tube was purged with argon and sealed, and the mixture was heated at ~140 °C until analytical TLC indicated full conversion (~3h). After cooling to rt, the reaction mixture was poured into water (~50 mL), stirred for 30 min and diluted with EtOAc (~100 mL). The organic phase was washed with water (4 × 50 mL), evaporated to dryness and the resulting crude purified by silica gel

column chromatography (2-4%, MeOH in CH<sub>2</sub>Cl<sub>2</sub>, v/v) to afford a residue, which was further purified through precipitation from refluxing methanol (30 min) to afford nucleoside **2** (yield specified below).

**2'-O-(Pyren-2-yl)methyl-uridine (2Y)**. O<sub>2</sub>,O<sub>2</sub>'-Anhydrouridine **1** (1.00 g, 4.42 mmol), 2-pyrenemethanol (2.05g, 8.84 mmol), NaHCO<sub>3</sub> (74.3 mg, 0.88 mmol), BH<sub>3</sub> in THF (2.21 mL, 2.21 mmol) and anhydrous DMSO (8 mL) were mixed, reacted, worked up, and purified as described above to afford nucleoside **2Y** (0.60 g, 30 %) as a white solid material. *R*<sub>f</sub>: 0.4 (10 % MeOH in CH<sub>2</sub>Cl<sub>2</sub>, v/v); MALDI-HRMS *m/z* 481.1386 ([M+Na]<sup>+</sup>, C<sub>26</sub>H<sub>22</sub>N<sub>2</sub>O<sub>6</sub>·Na<sup>+</sup>, Calc. 481.1370; <sup>1</sup>H NMR (DMSO-*d*<sub>6</sub>)<sup>35</sup>: δ 11.38 (s, 1H, ex, NH), 8.28-8.30 (d, 2H, *J* = 7.8 Hz, H<sub>6</sub><sub>Py</sub>, H<sub>8</sub><sub>Py</sub>), 8.23 (s, 2H, H<sub>1</sub><sub>Py</sub>, H<sub>3</sub><sub>Py</sub>), 8.17-8.20 (d, 2H, *J* = 8.8 Hz, H<sub>4</sub><sub>Py</sub>, H<sub>10</sub><sub>Py</sub>), 8.10-8.13 (d, 2H, *J* = 8.8 Hz, H<sub>5</sub><sub>Py</sub>, H<sub>9</sub><sub>Py</sub>), 8.07 (t, 1H, *J* = 7.8 Hz, H<sub>7</sub><sub>Py</sub>), 7.85 (d, 1H, *J* = 8.0 Hz, H<sub>6</sub>), 6.09 (d, 1H, *J* = 4.9 Hz, H<sub>1</sub>'), 5.51 (d, 1H, *J* = 8.0 Hz, H<sub>5</sub>), 5.35 (d, 1H, ex, *J* = 5.7 Hz, 3'-OH), 5.16-5.19 (d, 1H, *J* = 12.7 Hz, CH<sub>2</sub>Py), 5.11 (t, 1H, ex, *J* = 4.9 Hz, 5'-OH), 5.03-5.06 (d, 1H, *J* = 12.7 Hz, CH<sub>2</sub>Py), 4.23-4.26 (m, 1H, H<sub>3</sub>'), 4.12-4.15 (m, 1H, H<sub>2</sub>'), 3.98-4.00 (m, 1H, H<sub>4</sub>'), 3.65-3.69 (m, 1H, H<sub>5</sub>'), 3.57-3.62 (m, 1H, H<sub>5</sub>'); <sup>13</sup>C NMR (DMSO-*d*<sub>6</sub>): δ 163.0, 150.6, 140.2 (C<sub>6</sub>), 136.3, 130.54, 130.50, 127.5 (C<sub>4</sub><sub>Py</sub>, C<sub>10</sub><sub>Py</sub>), 127.2 (C<sub>5</sub><sub>Py</sub>, C<sub>9</sub><sub>Py</sub>), 126.1 (C<sub>7</sub><sub>Py</sub>), 125.1 (C<sub>6</sub><sub>Py</sub>, C<sub>8</sub><sub>Py</sub>), 123.7 (C<sub>1</sub><sub>Py</sub>, C<sub>3</sub><sub>Py</sub>), 123.2, 101.8 (C<sub>5</sub>), 86.4 (C<sub>1</sub>'), 85.2 (C<sub>4</sub>'), 80.8 (C<sub>2</sub>'), 71.3 (CH<sub>2</sub>Py), 68.4 (C<sub>3</sub>'), 60.5 (C<sub>5</sub>').

**2'-O-(Pyren-4-yl)methyl-uridine (2Z)**. O<sub>2</sub>,O<sub>2</sub>'-Anhydrouridine **1** (0.50 g, 2.21 mmol), 4-pyrenemethanol (1.03 g, 4.42 mmol), NaHCO<sub>3</sub> (37.1 mg, 0.44 mmol), BH<sub>3</sub> in THF (1.10 mL, 1.10 mmol) and anhydrous DMSO (5 mL) were mixed, reacted, worked up, and purified as described above to afford nucleoside **2Y** (200 mg, 20 %) as a white solid. *R*<sub>f</sub>: 0.4 (10 % MeOH in

CH<sub>2</sub>Cl<sub>2</sub>, v/v); MALDI-HRMS  $m/z$  481.1399 ([M+Na]<sup>+</sup>, C<sub>26</sub>H<sub>22</sub>N<sub>2</sub>O<sub>6</sub>Na<sup>+</sup>, Calc. 481.1370; <sup>1</sup>H NMR (DMSO-*d*<sub>6</sub>):  $\delta$  11.28 (s, 1H, ex, NH), 8.42 (d, 1H,  $J = 7.8$  Hz, Py), 8.29-8.31 (m, 2H, Py), 8.24-8.26 (d, 1H,  $J = 7.3$  Hz, Py), 8.18-8.22 (m, 3H, Py), 8.07 (t, 1H,  $J = 7.5$  Hz, Py), 8.03 (dd, 1H,  $J = 7.8$  Hz, 7.5 Hz, Py), 7.77 (d, 1H,  $J = 8.0$  Hz, H6), 6.08 (d, 1H,  $J = 5.4$  Hz, H1'), 5.39-5.43 (m, 3H, 1 ex, 3'-OH, H5 and CH<sub>2</sub>Py), 5.21-5.24 (d, 1H,  $J = 12.5$  Hz, CH<sub>2</sub>Py), 5.09 (t, 1H, ex, 5'-OH), 4.29-4.33 (m, 1H, H3'), 4.20-4.23 (m, 1H, H2'), 3.97-4.00 (m, 1H, H4'), 3.63-3.68 (m, 1H, H5'), 3.57-3.62 (m, 1H, H5'); <sup>13</sup>C NMR (DMSO-*d*<sub>6</sub>):  $\delta$  162.8, 150.5, 140.0 (C6), 132.8, 130.8, 130.5, 129.9, 129.0, 127.5 (Py), 127.0 (Py), 126.9 (Py), 126.3 (Py), 125.9 (Py), 125.3 (Py), 125.2 (Py), 124.1, 123.5, 121.7 (Py), 101.6 (C5), 86.0 (C1'), 85.4 (C4'), 80.7 (C2'), 70.2 (CH<sub>2</sub>Py), 68.4 (C3'), 60.6 (C5').

**General O5'-DMTr-protection protocol for the preparation of 3Y/3Z (description for ~1 mmol scale).** The appropriate nucleoside **2** (specific quantities given below) was co-evaporated twice with anhydrous pyridine and redissolved in anhydrous pyridine. To this was added 4,4'-dimethoxytritylchloride (DMTrCl) and catalytic *N,N*-dimethyl-4-aminopyridine (DMAP), and the reaction mixture was stirred at rt under an argon atmosphere until TLC indicated complete conversion (~14h). The reaction mixture was diluted with CH<sub>2</sub>Cl<sub>2</sub> (40 mL) and the organic phase was sequentially washed with water (2 × 30 mL) and sat. aq. NaHCO<sub>3</sub> (2 × 50 mL). The organic phase was evaporated to near dryness and the resulting crude co-evaporated with abs. EtOH and toluene (2:1, v/v, 3 × 3 mL) and purified by silica gel column chromatography (0-5%, MeOH in CH<sub>2</sub>Cl<sub>2</sub>, v/v) to afford nucleoside **3** (yield specified below).

**5'-O-(4,4'-Dimethoxytrityl)-2'-O-(pyren-2-yl)methyl-uridine (3Y).** Nucleoside **2Y** (500 mg, 1.09 mmol), DMTrCl (0.64 g, 1.63 mmol) and DMAP (~9 mg) in anhydrous pyridine (10 mL) were mixed, reacted, worked up and purified as described above to afford **3Y** (0.57 g, 68 %) as a pale yellow foam.  $R_f$ : 0.6 (5% MeOH in CH<sub>2</sub>Cl<sub>2</sub>, v/v); MALDI-HRMS  $m/z$  783.2706 ([M+Na]<sup>+</sup>, C<sub>47</sub>H<sub>40</sub>N<sub>2</sub>O<sub>8</sub>·Na<sup>+</sup>, Calc. 783.2677); <sup>1</sup>H NMR (DMSO-*d*<sub>6</sub>)<sup>35</sup>:  $\delta$  11.43 (s, 1H, ex, NH), 8.27-8.31 (m, 4H, H1<sub>Py</sub>, H3<sub>Py</sub>, H6<sub>Py</sub>, H8<sub>Py</sub>), 8.17-8.20 (d, 2H,  $J$  = 8.9 Hz, H4<sub>Py</sub>, H10<sub>Py</sub>), 8.11-8.13 (d, 2H,  $J$  = 8.9 Hz, H5<sub>Py</sub>, H9<sub>Py</sub>), 8.07 (t, 1H,  $J$  = 7.5 Hz, H7<sub>Py</sub>), 7.67 (d, 1H,  $J$  = 8.0 Hz, H6), 7.31-7.33 (m, 2H, DMTr), 7.22-7.26 (m, 2H, DMTr), 7.15-7.20 (m, 5H, DMTr), 6.78-6.84 (m, 4H, DMTr), 6.07-6.08 (d, 1H,  $J$  = 3.9 Hz, H1'), 5.45 (d, 1H, ex,  $J$  = 6.7 Hz, 3'-OH), 5.13-5.23 (m, 3H, H5, CH<sub>2</sub>Py), 4.31-4.35 (m, 1H, H3'), 4.18-4.20 (m, 1H, H2'), 4.09-4.12 (m, 1H, H4'), 3.68 (s, 3H, CH<sub>3</sub>O), 3.65 (s, 3H, CH<sub>3</sub>O), 3.30-3.34 (m, 1H, H5'; overlap with H<sub>2</sub>O), 3.23-3.26 (m, 1H, H5'); <sup>13</sup>C NMR (DMSO-*d*<sub>6</sub>):  $\delta$  162.9, 158.1, 158.0, 150.4, 144.4, 140.1 (C6), 136.2, 135.3, 135.0, 130.6, 130.5, 129.7 (DMTr), 129.6 (DMTr), 127.8 (DMTr), 127.6 (DMTr), 127.5 (Py), 127.2 (Py), 126.7 (Py), 126.1 (Py), 125.1 (Py), 123.68, 123.66 (Py), 123.2, 113.2 (DMTr), 113.1 (DMTr), 101.5 (C5), 87.2 (C1'), 85.9, 82.9 (C4'), 80.6 (C2'), 71.3 (CH<sub>2</sub>Py), 68.7 (C3'), 62.7 (C5'), 54.94 (CH<sub>3</sub>O), 54.92 (CH<sub>3</sub>O). A minor impurity of chloroform at 79.1 ppm was identified in the <sup>13</sup>C NMR.

**5'-O-(4,4'-Dimethoxytrityl)-2'-O-(pyren-4-yl)methyl-uridine (3Z).** Nucleoside **2Z** (150 mg, 0.33 mmol), DMTrCl (191 mg, 0.49 mmol) and DMAP (~4 mg) in anhydrous pyridine (5 mL) were mixed, reacted, worked up and purified as described above to afford **3Z** (200 mg, 80 %) as a pale yellow foam.  $R_f$ : 0.6 (5% MeOH in CH<sub>2</sub>Cl<sub>2</sub>, v/v); MALDI-HRMS  $m/z$  783.2695 ([M+Na]<sup>+</sup>, C<sub>47</sub>H<sub>40</sub>N<sub>2</sub>O<sub>8</sub>·Na<sup>+</sup>, Calc. 783.2677); <sup>1</sup>H NMR (DMSO-*d*<sub>6</sub>)<sup>36</sup>:  $\delta$  11.36 (s, 1H, ex, NH),



8.45 (d, 1H,  $J = 7.8$  Hz, Py), 8.17-8.33 (m, 6H, Py), 8.05 (t, 2H, H<sub>2Py</sub>, H<sub>7Py</sub>), 7.60 (d, 1H,  $J = 8.2$  Hz, H<sub>6</sub>), 7.30-7.32 (m, 2H, DMTr), 7.17-7.25 (m, 7H, DMTr), 6.78-6.84 (m, 4H, DMTr), 6.07 (d, 1H,  $J = 4.1$  Hz, H<sub>1'</sub>), 5.49 (d, 1H,  $J = 6.2$  Hz, ex, 3'-OH), 5.44-5.46 (m, 1H,  $J = 12.7$  Hz, CH<sub>2</sub>Py), 5.30-5.34 (d, 1H,  $J = 12.7$  Hz, CH<sub>2</sub>Py), 5.08 (d, 1H,  $J = 8.2$  Hz, H<sub>5</sub>), 4.38-4.42 (m, 1H, H<sub>3'</sub>), 4.26-4.28 (m, 1H, H<sub>2'</sub>), 4.09-4.12 (m, 1H, H<sub>4'</sub>), 3.71 (s, 3H, CH<sub>3</sub>O), 3.69 (s, 3H, CH<sub>3</sub>O), 3.30-3.34 (m, 1H, H<sub>5'</sub> – partial overlap with H<sub>2</sub>O), 3.22-3.25 (m, 1H, H<sub>5'</sub>); <sup>13</sup>C NMR (DMSO-*d*<sub>6</sub>):  $\delta$  162.8, 158.1, 158.0, 150.4, 144.4, 140.0 (C<sub>6</sub>), 135.3, 135.0, 132.7, 130.9, 130.5, 129.9, 129.7 (DMTr), 129.6 (DMTr), 129.0, 127.8 (DMTr), 127.6 (DMTr), 127.5 (Py), 127.1 (Py), 126.8 (Py), 126.7 (DMTr), 126.3 (C<sub>2Py</sub>), 126.0 (C<sub>7Py</sub>), 125.29 (Py), 125.25 (Py), 124.1, 123.5, 121.7 (Py), 113.2 (DMTr), 113.1 (DMTr), 101.4 (C<sub>5</sub>), 86.9 (C<sub>1'</sub>), 85.9, 83.2 (C<sub>4'</sub>), 80.5 (C<sub>2'</sub>), 70.2 (CH<sub>2</sub>Py), 68.7 (C<sub>3'</sub>), 62.8 (C<sub>5'</sub>), 55.0 (CH<sub>3</sub>O).

**General O3'-phosphitylation protocol for the preparation of 4Y and 4Z (description for ~0.25 mmol scale).** The appropriate nucleoside **3** (specific quantities given below) was co-evaporated with anhydrous 1,2-dichloroethane and redissolved in anhydrous CH<sub>2</sub>Cl<sub>2</sub>. To this was added *N,N*-diisopropylethylamine (DIPEA) and 2-cyanoethyl-*N,N*-diisopropylchlorophosphoramidite (PCI-reagent) and the reaction mixture was stirred at rt under an argon atmosphere until TLC indicated complete conversion (~3h), whereupon abs. EtOH (0.3 mL) and CH<sub>2</sub>Cl<sub>2</sub> (5 mL) were sequentially added. The organic phase was washed with sat. aq. NaHCO<sub>3</sub> (2 mL), evaporated to near dryness, and the resulting residue purified by silica gel column chromatography (40-70% EtOAc in petroleum ether, v/v) to afford phosphoramidite **4** (yield specified below).

**3'-O-(2-Cyanoethoxy(diisopropylamino)phosphinyl)-5'-O-(4,4'-dimethoxytrityl)-2'-O-(pyren-2-yl)methyl-uridine (4Y).** Nucleoside **3Y** (145 mg, 0.19 mmol), DIPEA (136  $\mu$ L, 0.76 mmol) and PCI-reagent (85  $\mu$ L, 0.38 mmol) in anhydrous  $\text{CH}_2\text{Cl}_2$  (5 mL) were mixed, reacted, worked up and purified as described above to afford phosphoramidite **4Y** (170 mg, 93 %) as a white foam.  $R_f$ : 0.8 (5% MeOH in  $\text{CH}_2\text{Cl}_2$ , v/v); MALDI-HRMS  $m/z$  983.3746 ( $[\text{M}+\text{Na}]^+$ ,  $\text{C}_{56}\text{H}_{57}\text{N}_4\text{O}_9\text{PNa}^+$ , Calc. 983.3755);  $^{31}\text{P}$  NMR ( $\text{CDCl}_3$ ):  $\delta$  150.5, 150.2.

**3'-O-(2-Cyanoethoxy(diisopropylamino)phosphinyl)-5'-O-(4,4'-dimethoxytrityl)-2'-O-(pyren-4-yl)methyl-uridine (4Z).** Nucleoside **3Z** (190 mg, 0.25 mmol), DIPEA (178  $\mu$ L, 0.99 mmol) and PCI-reagent (111  $\mu$ L, 0.49 mmol) in anhydrous  $\text{CH}_2\text{Cl}_2$  (5 mL) were mixed, reacted, worked up and purified as described above to afford phosphoramidite **4Z** (220 mg, 92 %) as a white foam.  $R_f$ : 0.8 (5% MeOH in  $\text{CH}_2\text{Cl}_2$ , v/v); MALDI-HRMS  $m/z$  983.3766 ( $[\text{M}+\text{Na}]^+$ ,  $\text{C}_{56}\text{H}_{57}\text{N}_4\text{O}_9\text{PNa}^+$ , Calc. 983.3755);  $^{31}\text{P}$  NMR ( $\text{CDCl}_3$ )  $\delta$  150.1, 150.0.

**Protocol - synthesis and purification of ONs.** Synthesis of **Y/Z**-modified ONs was performed on an automated DNA synthesizer using 0.2  $\mu$ mol scale succinyl linked LCAA-CPG (long chain alkyl amine controlled pore glass) columns with a pore size of 500 $\text{\AA}$ . Standard protocols for incorporation of DNA phosphoramidites were used. A ~50-fold molar excess of modified phosphoramidites in anhydrous acetonitrile (at 0.05 M), along with extended oxidation (45s) and coupling times (activator: 0.01 M 4,5-dicyanoimidazole, 15 min) was used during hand-couplings, which resulted in stepwise coupling yields of **4Y** and **4Z** of ~99% and ~98%, respectively. Cleavage from solid support and removal of protecting groups was accomplished upon treatment with 32% aq. ammonia (55  $^\circ\text{C}$ , 24 h). The crude ONs were purified via ion-pair

reverse phase HPLC (XTerra MS C18 column) using 0.05 M triethylammonium acetate - water/acetonitrile gradient, followed by detritylation (80% aq. AcOH, 20 min), and precipitation (NaOAc/NaClO<sub>4</sub>/acetone, -18 °C for 12-16 h). The identity of synthesized ONs was established through MALDI-MS analysis (Table S1) recorded in positive ions mode on a Quadrupole Time-Of-Flight Tandem Mass Spectrometer (Q-TOF Premiere) equipped with a MALDI source (Waters Micromass LTD., U.K) using anthranilic acid as a matrix, while purity (>85%) was verified by ion-pair reverse phase HPLC running in analytical mode.

**Protocol - thermal denaturation studies.** Concentrations of ONs were estimated using the following extinction coefficients for DNA (OD/μmol): G (12.01), A (15.20), T (8.40), C (7.05); for RNA (OD/μmol): G (13.70), A (15.40), U (10.00), C (9.00); for pyrene (OD/μmol): (22.4)<sup>31</sup> Strands were thoroughly mixed and denatured by heating to 70-85 °C, followed by cooling to the starting temperature of the experiment. Quartz optical cells with a path length of 1.0 cm were used. Thermal denaturation temperatures ( $T_m$ 's) of duplexes (1.0 μM final concentration of each strand) were measured on a Cary 100 UV/VIS spectrophotometer equipped with a 12-cell Peltier temperature controller and determined as the maximum of the first derivative of the thermal denaturation curve ( $A_{260}$  vs.  $T$ ) recorded in medium salt buffer ( $T_m$  buffer: 100 mM NaCl, 0.1 mM EDTA, and pH 7.0 adjusted with 10 mM Na<sub>2</sub>HPO<sub>4</sub> and 5 mM Na<sub>2</sub>HPO<sub>4</sub>). The temperature of the denaturation experiments ranged from at least 15 °C below  $T_m$  to 20 °C above  $T_m$  (although not below 3 °C). A temperature ramp of 0.5 °C/min was used in all experiments. Reported  $T_m$ -values are averages of two experiments within  $\pm 1.0$  °C.

**Protocol - determination of thermodynamic parameters.** Thermodynamic parameters for duplex formation were determined through baseline fitting of denaturation curves (van't Hoff analysis) using software provided with the UV/VIS spectrometer. Bimolecular reactions, two-state melting behavior, and a heat capacity change of  $\Delta C_p = 0$  upon hybridization were assumed.<sup>30</sup> A minimum of two experimental denaturation curves were each analyzed at least three times to minimize errors arising from baseline choice. Averages and standard deviations are listed.

**Protocol – absorption spectra.** UV-vis absorption spectra (range: 300-400 nm) were recorded at 5 °C using the same samples and instrumentation as in the thermal denaturation experiments.

**Protocol - steady-state fluorescence emission spectra.** Steady-state fluorescence emission spectra of ONs modified with pyrene-functionalized monomers **X-Z** and the corresponding duplexes with complementary DNA/RNA targets, were recorded in non-deoxygenated thermal denaturation buffer (each strand at 1.0  $\mu$ M concentration) and obtained as an average of five scans using an excitation wavelength of  $\lambda_{ex} = 350, 345$  or  $340$  nm for **X**-, **Y**- or **Z**-modified ONs, excitation slit 5.0 nm, emission slit 2.5 nm and a scan speed of 600 nm/min. Experiments were determined at 5 °C to ascertain maximal hybridization of probes to DNA/RNA targets (a stream of nitrogen was blown in to the chamber to prevent condensation).

**Protocol - molecular modeling.** The initial structures of the **X/Y/Z**-modified DNA duplexes were generated by building and modifying a standard *B*-type DNA duplex using MacroModel v9.8.<sup>37</sup> The charge of the phosphodiester backbone was neutralized with sodium ions, which

were placed 3.0 Å from non-bridging oxygen atoms and restrained to this distance by a force constant of 100 kJ·mol<sup>-1</sup>·Å<sup>-2</sup>. A preliminary minimization was carried out using the Polak-Ribiere conjugate gradient method (convergence criteria 0.1 kJ·mol<sup>-1</sup>·Å<sup>-1</sup>), the AMBER94 force field<sup>38</sup> with the improved parambsc0 parameter set,<sup>39</sup> and the implicit GB/SA continuum solvation model<sup>40</sup> as implemented in MacroModel v9.8; all atoms were frozen except those in the O2'-substituent of the modified monomers. Non-bonded interactions were treated with extended cut-offs (van der Waals 8.0 Å and electrostatics 20.0 Å).

The seed structure for **X2:D4** was generated by taking previously reported NMR data on **X**-modified DNA duplexes into account.<sup>31</sup> Thus, distances between atoms for which NOE contacts have been reported were constrained to 3.0-5.0 Å by a force constant of 100 kJ·mol<sup>-1</sup>·Å<sup>-2</sup> (i.e., distances between i) pyrene and H5 of the modified uridine, ii) pyrene and H2/H8 of the 3'-flanking adenosine, and iii) pyrene and H6 of the thymine opposite of the 3'-flanking adenosine). The structure was minimized as described above with the following considerations: i) all atoms were allowed to move freely during minimization, ii) sodium ions were restrained as above, and iii) hydrogen bonding of the outermost base pairs were restrained by a force constant of 100 kJ·mol<sup>-1</sup>·Å<sup>-2</sup> ((C)2-O···HN-2(G), distance 1.99 Å, (C)N3···H-N1(G), distance 1.90 Å and (C)4-NH···O-6(G), distance 1.69 Å). The resulting lowest energy structure formed the basis for construction of the seed structures for all other studied duplexes. Pyrene moieties of the other duplexes were manually adjusted to intercalated positions and the duplexes minimized as described for **X2:D4**. Seed structures were then submitted to 5 ns of stochastic dynamics (simulation temperature 300 K, time step 2.2 fs, SHAKE all bonds to hydrogen) using the same constraints as employed above (except for NOE constraints), during which 1000

structures were sampled and subsequently minimized. The resulting structures were analyzed using MacroModel v9.8 and the 3DNA web server.<sup>41</sup>

**Protocol - electrophoretic mobility shift assay.** This assay was performed, essentially as previously described.<sup>13</sup> Unmodified DNA hairpins **DH1-DH7** were obtained from commercial sources and used without further purification. The DNA hairpins were 3'-DIG-labeled using the 2<sup>nd</sup> generation DIG Gel Shift Kit (Roche Applied Bioscience) as recommended by the manufacturer. DIG-labeled ONs obtained in this manner, were diluted and used without further purification in the recognition experiments. Pre-annealed probes (90 °C for 10 min, cooled to room temperature over 15 min) and DIG-labeled DNA hairpins (34.4 nM) were mixed and incubated in HEPES buffer (50 mM HEPES, 100 mM NaCl, 5 mM MgCl<sub>2</sub>, 10% sucrose, 1.44 mM spermine tetrahydrochloride, pH 7.2) for 15h at ambient temperature (~21±3 °C). The reaction mixtures were then diluted with 6x DNA loading dye (Fermentas) and loaded onto a 16% non-denaturing polyacrylamide gel. Electrophoresis was performed using a constant voltage of 70 V for 2h at ~4 °C. Gels were blotted onto a positively charged nylon membrane (Roche Applied Bioscience) using constant voltage with external cooling (100V, ~4 °C). The membranes were exposed to anti-digoxigenin-AP F<sub>ab</sub> fragments as recommend by the manufacturer of the DIG Gel Shift Kit, transferred to a hybridization jacket, and incubated with the substrate (CSPD) in detection buffer for 10 min at 37 °C. The chemiluminescence of the formed product was captured on X-ray film, which was developed using an X-Omatic 1000A X-ray film developer (Kodak). The resulting bands were quantified using a Fluor-S MultiImager (Bio-Rad, Hercules, CA) equipped with Quantity One software. Invasion efficiency was

determined as the intensity ratio between the recognition complex band and the total lane. An average of three independent experiments is reported along with standard deviations.

**Definition of zipper nomenclature.** The following nomenclature describes the relative arrangement between two monomers positioned on opposing strands in a duplex. The number  $n$  describes the distance measured in number of base pairs and has a positive value if a monomer is shifted toward the 5'-side of its own strand relative to a second reference monomer on the other strand. Conversely,  $n$  has a negative value if a monomer is shifted toward the 3'-side of its own strand relative to a second reference monomer on the other strand.

**Acknowledgements.** This study was supported by Award Number GM088697 from the National Institute of General Medical Sciences, National Institutes of Health; Awards IF13-001 and IF14-012 from the Higher Education Research Council, Idaho State Board of Education; The Office of Naval Research (N00014-10-1-0282); INBRE Program, NIH Grant Nos. P20 RR016454 (National Center for Research Resources) and P20 GM103408 (National Institute of General Medical Sciences); and Minitube of America. A.S.M is a Sapere Aude Postdoctoral Fellow (The Danish Council for Independent Research). We thank Dr. Lee Deobald (EBI Murdock Mass Spectrometry Center, Univ. Idaho) for assistance with mass spectrometric analysis, Prof. Carolyn Bohach (Food Science, Univ. Idaho) for access to gel documentation stations, and Prof. Jean'ne Shreeve (Dept. Chemistry, Univ. Idaho) for access to Parr reactors.

**Electronic supplementary information (ESI) available:** General experimental section; MS-data for modified ONs; representative thermal denaturation curves; additional denaturation and

thermodynamic data; additional absorption and steady-state fluorescence emission spectra; complete data set of structural parameters from modeling studies; lowest energy representations of Type B structures; NMR spectra for nucleosides **2Y-4Z**. See DOI:

### References and notes

<sup>a</sup> University of Idaho.

<sup>b</sup> Technical University of Denmark.

<sup>c</sup> Brigham Young University-Idaho.

1) J. D. Watson and F. H. C. Crick, *Nature*, 1953, **171**, 737-738.

2) (a) P. B. Dervan and B. S. Edelson, *Curr. Opin. Struct. Biol.*, 2003, **13**, 284-299; (b) M. S. Blackledge and C. Melander, *Bioorg. Med. Chem.*, 2003, **21**, 6101-6114.

3) (a) I. Ghosh, C. I. Stains, A. T. Ooi and D. J. Segal, *Mol. BioSyst.*, 2006, **2**, 551-560; (b) A. J. Bogdanove and D. F. Voytas, *Science*, 2011, **333**, 1843-1846; (c) T. Gaj, C. A. Gersbach, and C. F. Barbas III, *Trends Biotechnol.*, 2013, **31**, 397-405.

4) M. Duca, P. Vekhoff, K. Oussedik, L. Halby and P. B. Arimondo, *Nucleic Acids Res.*, 2008, **36**, 5123-5138.

5) (a) P. E. Nielsen, M. Egholm, R. H. Berg and O. Buchardt, *Science*, 1991, **254**, 1497-1500; (b) T. Bentin and P. E. Nielsen, *Biochemistry*, **1996**, *35*, 8863-8869; (c) K. Kaihatsu, D. A. Braasch, A. Cansizoglu and D. R. Corey, *Biochemistry*, 2002, **41**, 11118-11125; (d) K. Kaihatsu, B. A. Janowski and D. R. Corey, *Chem. Biol.*, 2004, **11**, 749-758.

6) For other groove-binding strategies see e.g., (a) W. C. Tse and D. L. Boger, *Chem. Biol.* 2004, **11**, 1607-1617; (b) P. L. Hamilton and D. P. Arya, *Nat. Prod. Rep.*, 2012, **29**, 134-143.



- 7) (a) T. Bentin, H. J. Larsen and P. E. Nielsen, *Biochemistry*, 2003, **42**, 13987-13995; (b) K. Kaihatsu, R. H. Shah, X. Zhao and D. R. Corey, *Biochemistry*, 2003, **42**, 13996-14003; (c) D. A. Horne and P. B. Dervan, *J. Am. Chem. Soc.*, 1990, **112**, 2435-2437; (d) V. V. Filichev, C. M. Nielsen, N. Bomholt, C. H. Jessen and E. B. Pedersen, *Angew. Chem. Int. Ed.*, 2006, **45**, 5311-5315; (e) D. A. Rusling, V. E. C. Powers, R. T. Ranasinghe, Y. Wang, S. D. Osborne, T. Brown and K. Fox, *Nucleic Acids Res.*, 2005, **33**, 3025-3032; (f) Y. Hari, S. Obika and T. Imanishi, *Eur. J. Org. Chem.*, 2012, 2875-2887.
- 8) (a) T. Ishihara and D. R. Corey, *J. Am. Chem. Soc.*, 1999, **121**, 2012-2020; (b) L. Milne, Y. Xu, D. M. Perrin and D. S. Sigman, *Proc. Natl. Acad. Sci. U.S.A.*, 2000, **97**, 3136-3141; (c) V. V. Filichev, B. Vester, L. H. Hansen and E. B. Pedersen, *Nucleic Acids Res.*, 2005, **33**, 7129-7137; (d) B. A. Janowski, K. Kaihatsu, K. E. Huffman, J. C. Schwartz, R. Ram, D. Hardy, C. R. Mendelson and D. R. Corey, *Nat. Chem. Biol.*, 2005, **1**, 210-215; (e) R. Beane, S. Gabillet, C. Montailier, K. Arar and D. R. Corey, *Biochemistry*, 2008, **47**, 13147-13149.
- 9) (a) I. V. Kutyavin, R. L. Rhinehart, E. A. Lukhtanov, V. V. Gorn, R. B. Meyer Jr. and H. B. Gamper Jr., *Biochemistry*, 1996, **35**, 11170-11176; (b) I. V. Smolina and V. V. Demidov, *Chem. Biol.*, 2003, **10**, 591-595.
- 10) (a) J. Lohse, O. Dahl and P. E. Nielsen, *Proc. Natl. Acad. Sci. U.S.A.*, 1999, **96**, 11804-11808; (b) T. Ishizuka, J. Yoshida, Y. Yamamoto, J. Sumaoka, T. Tedeschi, R. Corradini, S. Sforza and M. Komiyama, *Nucleic Acids Res.*, 2008, **36**, 1464-1471.
- 11) V. V. Demidov, E. Protozanova, K. I. Izvolsky, C. Price, P. E. Nielsen, M. D. Frank-Kamenetskii, *Proc. Natl. Acad. Sci. U.S.A.*, 2002, **99**, 5953-5958.
- 12) (a) S. Rapireddy, R. Bahal and D. H. Ly, *Biochemistry*, 2011, **50**, 3913-3918; (b) R. Bahal, B. Sahu, S. Rapireddy, C.-M. Lee and D. H. Ly, *ChemBioChem*, 2012, **13**, 56-60.

- 13) B. A. Didion, S. Karmakar, D. C. Guenther, S. Sau, J. P. Verstegen and P. J. Hrdlicka, *ChemBioChem*, 2013, **14**, 1534-1538.
- 14) D. M. Crothers, *Biopolymers*, 1968, **6**, 575-584.
- 15) (a) P. J. Hrdlicka, T. S. Kumar and J. Wengel, *Chem. Commun.*, **2005**, 4279-4281; (b) S. P. Sau, T. S. Kumar and P. J. Hrdlicka, *Org. Biomol. Chem.*, 2010, **8**, 2028-2036.
- 16) S. P. Sau, A. S. Madsen, P. Podbevsek, N. K. Andersen, T. S. Kumar, S. Andersen, R. L. Rathje, B. A. Anderson, D. C. Guenther, S. Karmakar, P. Kumar, J. Plavec, J. Wengel and P. J. Hrdlicka, *J. Org. Chem.*, 2013, **78**, 9560-9570.
- 17) (a) M. Nakamura, Y. Shimomura, Y. Ohtoshi, K. Sasa, H. Hayashi, H. Nakano and K. Yamana, *Org. Biomol. Chem.*, 2007, **5**, 1945-1951; (b) S. Karmakar, B. A. Anderson, R. L. Rathje, S. Andersen, T. Jensen, P. Nielsen and P. J. Hrdlicka, *J. Org. Chem.*, 2011, **76**, 7119-7131.
- 18) (a) T. S. Kumar, A. S. Madsen, M. E. Østergaard, S. P. Sau, J. Wengel and P. J. Hrdlicka, *J. Org. Chem.*, 2009, **74**, 1070-1081; (b) N. K. Andersen, B. A. Anderson, J. Wengel and P. J. Hrdlicka, *J. Org. Chem.*, 2013, **78**, 12690-12702.
- 19) S. Karmakar, D. C. Guenther and P. J. Hrdlicka, *J. Org. Chem.*, 2013, **78**, 12040-12048.
- 20) S. K. Roy and J. Y. Tang, *Org. Proc. Res. Dev.*, 2000, **4**, 170-171.
- 21) B. S. Ross, R. H. Springer, Z. Tortorici, and S. Dimock, *Nucleosides Nucleotides* 1997, **16**, 1641-1643.
- 22) 2-pyrenemethanol was obtained from pyrene according to: (a) V. V. Filichev, I. V. Astakhova, A. D. Malakhov, V. A. Korshun and E. B. Pedersen, *Chem. Eur. J.*, 2008, **14**, 9968-9980; (b) R. G. Harvey, S. Schmolka, C. Cortez and H. Lee, *Synth. Commun.*, 1988, **18**, 2207-

2209; (c) K. K. Laali and P. E. Hansen, *J. Org. Chem.*, 1997, **62**, 5804-5810. See Scheme S1 and the ESI<sup>†</sup> for further details.

23) 4-pyrenemethanol was obtained from pyrene according to reference 22a and (a) A. Streitwieser Jr., R. G. Lawler and D. Schwaab, *J. Org. Chem.*, 1965, **30**, 1470-1473; (b) M. Konieczny and R. G. Harvey, *J. Org. Chem.*, 1979, **44**, 2158-2160; (c) R. G. Harvey, M. Konieczny and J. Pataki, *J. Org. Chem.*, 1983, **48**, 2930-2932. See Scheme S2 and the ESI<sup>†</sup> for further details.

24) (a) K. Yamana, R. Iwase, S. Furutani, H. Tsuchida, H. Zako, T. Yamaoka and A. Murakami, *Nucleic Acids Res.*, 1999, **27**, 2387-2392; (b) M. Nakamura, Y. Fukunaga, K. Sasa, Y. Ohtoshi, K. Kanaori, H. Hayashi, H. Nakano and K. Yamana, *Nucleic Acids Res.*, 2005, **33**, 5887-5895.

(25) (a) U. B. Christensen and E. B. Pedersen, *Nucleic Acids Res.*, 2002, **30**, 4918-4925; (b) T. Bryld, T. Højland and J. Wengel, *Chem. Commun.*, 2004, 1064-1065.

(26) (a) V. A. Korshun, D. A. Stetsenko and M. J. Gait, *J. Chem. Soc. Perkin Trans. 1*, 2002, 1092-1104; (b) C. Dohno and I. Saito, *ChemBioChem*, 2005, **6**, 1075-1081.

(27) (a) G. Dougherty and J. R. Pilbrow, *Int. J. Biochem.*, 1984, **16**, 1179-1192; (b) H. Asanuma, T. Fujii, T. Kato and H. Kashida, *J. Photochem. Photobiol. C.*, 2012, **13**, 124-135.

(28) (a) M. Manoharan, K. L. Tivel, M. Zhao, K. Nafisi and T. L. Netzel, *J. Phys. Chem.*, 1995, **99**, 17461-17472; (b) Y. J. Seo, J. H. Ryu and B. H. Kim, *Org. Lett.*, 2005, **7**, 4931-4933; (c) J. N. Wilson, Y. Cho, S. Tan, A. Cuppoletti and E. T. Kool, *ChemBioChem* 2008, **9**, 279-285.

(29) For an overview of nucleic acid parameters, see: W. K. Olson, M. Bansal, S. K. Burley, R. E. Dickerson, M. Gerstein, S. C. Harvey, U. Heinemann, X.-J. Lu, S. Neidle, Z. Shakked, H. Sklenar, M. Suzuki, C.-S. Tung, E. Westhof, C. Wolberger and H. M. Berman, *J. Mol. Biol.*, 2001, **313**, 229-237.

- (30) J. L. Mergny and L. Lacroix, *Oligonucleotides*, 2003, **13**, 515-537.
- (31) (a) F. M. Winnik, *Chem. Rev.*, 1993, **93**, 587-614; (b) N. N. Dioubankova, A. D. Malakhov, D. A. Stetsenko, M. J. Gait, P. E. Volynsky, R. G. Efremov and V. A. Korshun, *ChemBioChem*, 2003, **4**, 841-847; (c) P. J. Hrdlicka, B. R. Babu, M. D. Sørensen and J. Wengel, *Chem. Commun.* 2004, 1478-1479; (d) F. Seela and S. A. Ingale, *J. Org. Chem.*, 2010, **75**, 284-295; (e) R. Haner, F. Garo, D. Wenger and V. L. Malinovskii, *J. Am. Chem. Soc.*, 2010, **132**, 7466-7471; (f) F. Wojciechowski, J. Lietard and C. J. Leumann, *Org. Lett.*, 2012, **14**, 5176-5179.
- (32) (a) I. V. Astakhova, A. D. Malakhov, I. A. Stepanova, A. V. Ustinov, S. L. Bondarev, A. S. Paramonov and V. A. Korshun, *Bioconj. Chem.*, 2007, **18**, 1972-1980; (b) I. V. Astakhova, A. V. Ustinov, V. A. Korshun and J. Wengel, *Bioconj. Chem.*, 2011, **22**, 533-539.
- 33) We use the DNA hairpin assay in lieu of footprinting experiments to avoid reliance on  $^{32}\text{P}$ -labelled targets. Moreover, linearized plasmids were not used as targets due to insufficient mobility differences on non-denaturing PAGE gels between recognition complexes and free linearized plasmids. We have previously demonstrated that the recognition complex between Invaders and DNA hairpins indeed is comprised of three strands as depicted in Figure 6a. Long incubation periods were chosen to ensure that equilibrium was reached. However, shorter incubation periods (<3h) can be used for biological applications see reference 13.
- 34) The assignment of C4/C5 and C9/C10 is interchangeable.
- 35) The assignments of H4<sub>Py</sub>/H10<sub>Py</sub> and H5<sub>Py</sub>/H9<sub>Py</sub> (and the corresponding  $^{13}\text{C}$  NMR signals) are interchangeable.
- 36) The assignments of H2<sub>Py</sub>/H7<sub>Py</sub> (and the corresponding  $^{13}\text{C}$  NMR signals) are interchangeable.
- 37) MacroModel, version 9.8, Schrödinger, LLC, New York, NY, **2010**.

- 38) W. D. Cornell, P. Cieplak, C. I. Bayly, I. R. Gould, K. M. Merz, D. M. Ferguson, D. C. Spellmeyer, T. Fox, J. W. Caldwell and P. A. Kollman, *J. Am. Chem. Soc.*, 1995, **117**, 5179-5197.
- 39) A. Pérez, I. Marchán, D. Svozil, J. Sponer, T. E. Cheatham, C. A. Laughton and M. Orozco, *Biophys. J.*, 2007, **92**, 3817-3829.
- 40) W. C. Still, A. Tempczyk, R. C. Hawley and T. Hendrickson, *J. Am. Chem. Soc.*, 1990, **112**, 6127-6129.
- 41) G. Zheng, X-J. Lu, W. K. Olson, *Nucleic Acids Res.* 2009, **37**, W240–W246.